Journal of Molecular Structure 1257 (2022) 132584

Contents lists available at ScienceDirect

Journal of Molecular Structure

journal homepage: www.elsevier.com/locate/molstr

Quercetin - based rhodium(III) complex: Synthesis, characterization and diverse biological potentials

Heba A. Sahyon[a], Fayez Althobaiti[b], Abd El-Motaleb M. Ramadan[a,*], Ahmed M. Fathy[c]

[a] Chemistry Department, Faculty of Science, Kafrelsheikh University, 33516 Kafrelsheikh, Egypt
[b] Department of Biotechnology, College of Science, Taif University, P.O. Box 11099, Taif 21944, Saudi Arabia
[c] Chemistry Department, Faculty of Science, Zagazig University, Zagazig, Egypt

ARTICLE INFO

Article history:
Received 13 November 2021
Revised 29 January 2022
Accepted 4 February 2022
Available online 5 February 2022

Keywords:
Quercetin
Rhodium(III)
Biomimicking
SOD
DNA binding
Caspase9
MMP9

ABSTRACT

Quercetin – based rhodium(III) complex, [$Rh^{III}L_2ClH_2O$], L is quercetin, was synthesized via the direct interaction between the polyphenolic natural product (3,3′,4′,5,7-pentahydroxylflavone) and $RhCl_3$ $3H_2O$. Characterization of the pure isolated metal complex by analytical, electrolytic conductance, TGA and spectroscopic techniques demonstrated the stoichiometric ratio 1:2 metal to ligand. The final structure of [$Rh^{III}L_2ClH_2O$] was confirmed using PXRD–structural analysis by processing the XRD data of microcrystalline powder by the relevant computer program Expo 2014. The mimetic catalytic activity of superoxide dismutase (SOD) was studied and the obtained results showed that [$Rh^{III}L_2ClH_2O$] has mid activity compared to other SOD mimics. By analogy with the work of the original-SOD and its functional models, a mechanism for SOD-mimicking catalytic activity of the newly synthesized rhodium(III) complex has been proposed. The binding of the Rh(III) chelate to DNA was tested, and spectroscopic investigations indicated the successful binding of the metal complex to DNA by the groove/electrostatic binding pattern with intrinsic binding constants K_b of 2.76×10^6 M^{-1}. In addition, the quercetin – based Rh^{III} exhibits relatively higher DPPH scavenger power than the free quercetin. The *in vitro* data indicated the efficient anti-proliferative activities of the current rhodium(III) complex compared with cis-platin with increased safety on normal cells. In addition, our data revealed that the studied Rh^{III} complex could prevent cancer cell replication with increasing the p53 levels, inhibit both *Bcl2* and MMP9, then activating caspase 9, which then cleaves caspase 3, leading to apoptosis triggering. Apoptosis activation led to cell cycle arrest at the pre-G1 phase and decreased Hela cell proliferation, which appeared in the decreased G2/M phase. Ongoing biological assays indicate that the current Rh(III) complex is a promising anti-proliferative agent with minimal toxicity to normal cells.

1. Introduction

Cisplatin was discovered in 1965 and is clinically considered the most successful anticancer agent against several cancer types [1–4]. Up till now, cisplatin was clinically used in limited cases with plenty of side effects, such as nephrotoxicity, cardiotoxicity, and the appearance of drug resistance cancers [5–7]. As a result of these toxicities, scientists have to innovate other non-platinum anticancer drugs with reduced side effects, such as ruthenium [8,9] and rhodium [10–13]. Although hexa-coordinated low-spin rhodium(III) complexes with the electronic configuration ($t_{2g}^6e_g^0$) is kinetically inert, some Rh^{III} - based complexes have been shown to have significant anticancer activities [12–14]. However, rhodium(III) ion forms biologically active and stable complexes with multiple ligands [15–17]. These rhodium(III) complexes were proven to have other antitumor pathways, such as binding to DNA mismatches [10,18–20] rather than disturbing the double helix structure as cisplatin. In this context, the cancer cell's mitochondria is aiming to produce apoptotic death by increasing their free radical levels [21]. Recently, a Rh^{III} - based complex was successfully prepared and established to induce malignant cell apoptosis through induction of caspases with decreasing the *Bcl2* expression through increased free radicals [13].

Quercetin is a popular, edible Flavonoid found in vegetables and fruits with marked antioxidant and anticancer activities [22–29]. The structure of quercetin, with its phenolic OH groups, shows a remarkable ability to react with transition metal ions to form stable metal chelates [30,31]. Recently, the ability of quercetin to form stable complexes with ruthenium, calcium, magnesium, zinc, iron, copper, and aluminum has been confirmed [32–35]. Most

* Corresponding author.
E-mail address: Ramadanss@hotmail.com (A.E.M. Ramadan).

https://doi.org/10.1016/j.molstruc.2022.132584
0022-2860/

quercetin-based metal complexes showed higher antioxidant and anticancer activities than quercetin itself [32–35].

The superoxide anion radical ($O_2^{\bullet-}$), a by-product from energy production processes by O_2, is the origin of the formation of the reactive oxygen species (ROS), which are extremely harmful to all aerobic organisms. Native SOD-proteins including CuZn-SOD, Mn-SOD, Fe-SOD and Ni-SOD rid the cell of $O_2^{\bullet-}$ accumulation. The therapeutic use of natural SOD proteins faced many complications, such as cell wall permeability, immune problems, and reduced shelf life, which precluded their use as drugs. These concerns, combined with the lack of clinical success with natural SOD-enzymes, have motivated efforts to develop synthetic alternatives such as transition metal complexes as functional models for SOD-proteins. Several SOD-mimics have been synthesized with different transition metals such as copper, manganese, iron and nickel and most of them have demonstrated high efficiency [36,37]. With regard to rhodium(III) complexes, there are no studies in the literature yet regarding their use as SOD-mimetics.

To our knowledge, the metal complex of rhodium(III) with quercetin has not yet been reported. The present work aims to synthesize a quercetin – based Rh(III) complex to examine its *in vitro* antioxidant and anticancer activities and compare it with free quercetin. Superoxide dismutase-like activity, DNA binding, cell death mode and proposed anticancer mechanism of quercetin–based Rh^{III} complex will be investigated.

2. Experimental

2.1. Chemicals

Dimethyl sulfoxide (DMSO), MTT [3-(4,5-dimethylthiazol-2-yl)−2,5-diphenyltetrazolium bromide], Nitroblue tetrazolium (NBT), NADH, phenazine methosulphate (PMS), 2,2-Diphenyl-1-picrylhydrazyl (DPPH), rhodium(III) chloride trihydrate and sodium pyrophosphate decahydrate were purchased from Sigma-Aldrich, St. Louis, MO, USA, Fetal Bovine serum and penicillin/streptomycin were obtained from GIBCO, UK. Trypsin 0.25% (AMRESCO - USA). The human cell lines; hepatocellular carcinoma (HepG-2), epitheliod carcinoma (Hela), mammary carcinoma (MCF-7), human prostate cancer (PC-3), colorectal adenocarcinoma (Caco-2) and human lung fibroblast (WI38) were obtained from American Type Culture Collection (ATCC, NY, USA) via Holding company for biological products and vaccines (VACSERA), Cairo, Egypt. Quercetin dihydrate **[**($C_{15}H_{10}O_7$ $2H_2O$) 97% Lot.no. 10,181,203, Alfa Caesar Company, Germany**]**, Dulbeco's Modified Eagle's Medium (DMEM) (GIBCO, New York, USA; Cat.no.11995073), fetal bovine serum (GIBCO, Grand Island, New York, USA;Cat.no.10099133), L-glutamine (Invitrogen, Grand Island, New York, USA; Cat.no. 25,030,024), ethidium bromide and acridine orange (EB/AO) (Sigma-Aldrich, Deisenhofen, Germany). Annexin V kit (cat. No. 556,547 BD Pharmingen FITC apoptosis kit) was purchased from Becton, Dickinson and Company. Anti-rabbit antibodies (polyclonal Ig) for anti-caspase-9 antibody ([2–22] ab69541), anti-MMP9 antibody (ab73734), *Bcl2* anti-mouse (ab196495), β-actin (monoclonal Ig) (ab6276) were obtained from BD Abcam. The chemiluminescent western blot ECL substrate reagent was obtained from Perkin Elmer, Waltham, MA, USA. Qiagen RNA extraction kits, BioRad syber green PCR MMX. All chemicals used in the current study are of the analytical grade and used without further purification.

2.2. Characterization techniques

Characterization techniques were performed as described in the supplementary materials S1. As well, the experimental details of superoxide dismutase biomimetic catalytic activity, SOD levels in the treated/untreated Hela cells, and the DNA binding assay are included in S1.

2.3. Synthesis of quercetin – based rhodium(III) complex

Quercetin powder 0.002 mole was dissolved in a 50 mL alcoholic solution containing 0.002 mole of NaOH. To this solution 0.001 mole of $RhCl_3$ $3H_2O$ dissolved in EtOH was added drop by drop with stirring. The resulting mixture then was stirred at 25 °C for 30 min., during which the metal complex was formed in a dissolved form. By slow evaporation of the reaction mixture a dark red microcrystalline precipitate formed. The colored precipitated residue was separated by filtration and washed with small portions of a mixture of EtOH and diethyl ether (1:1) numerous times and then was left to dry under anhydrous conditions for 1 week.

2.4. Biological examinations

2.4.1. DPPH test

Serial dilutions (200–10 µg/mL) of both quercetin and quercetin – based Rh^{III} complex were mixed with DPPH reagent, then incubated and measured as mentioned in our pervious study [38]. Reduced absorbance values showed greater free radical scavenging activity. All analyses were achieved in triplicate. To calculate the sample concentration which prevents the 50% from the color formed by the DPPH radical, a curve was plotted between the concentration and color intensity and the IC_{50} value was calculated from it [39].

2.4.2. In vitro anticancer activity of quercetin–based rhodium(III) complex

To identify the anticancer activity of the newly synthesized quercetin-based rhodium(III) complex against human cancer cell proliferation, the MTT assay was done [40], as described in the supplementary data S1.

2.4.3. Flowcytometric determination

2.4.3.1. Annexin and Pi assay for apoptosis determination. The Hela cells treated with IC_{50} of quercetin- based rhodium(III) complex were suspended in cold PBS, centrifuged in a cooling centrifuge at 2000 rpm for 30 min. The separated pellet was then transmitted into a sterilized plain tube. Finally, the annexin V kit (Cat. No.556547 BD pharmingen FITC apoptosis Kit) was used to stain the pellet, as reported in our previous study [38].

2.4.3.2. Cell cycle examination. The Hela cells treated with 9.40 µg/ml of the quercetin–based-rhodium(III) complex was incubated in the CO_2 incubator for 48 h. Then further steps was done to the treated/untreated cells as mentioned in our previous work [9]. The cells were then examined using a BD FACSCalibur flow cytometer (Becton Dickinson, Sunnyvale, CA, USA). The treated and untreated Hela cells tubes were covered with dark foil and preserved for 12 h in dark place to be analysed by the flow-cytometer to examine the pre-G1 percentage.

2.5. Analysis of p53 genes by real-time PCR

RNA was extracted from the Hela cells treated with the quercetin–based-rhodium(III) complex as well as untreated Hela cells using the RNeasy Mini Kit (Qiagen, Germantown, MD, USA) according to the company's procedure. The expression level of P53 gene (F:5′-AGAGTCTATAGGCCCACCCC-3′ & R:5′-GCTCGACGCTAGGATCTGAC-3′), and housekeeping gene; *β-actin* (F: 5′-AGAGCTACGAGCTGCCTGAC-3′ & R: 5′-AGCACTGTGTTGGCGTACAG-3′) were assessed by real-time PCR.

Then further steps were done as mentioned in our previous work [9]. qPCR was done by QuantiTect SYBR Green qPCR Master Mix in a Step One Plus real-time PCR system as follows: the adjusted time for enzyme activation was 10 min at 95 °C followed by 40 cycles of 15 s at 95 °C, 20 s at 55 °C, and 30 s at 72 °C for the amplification step. The β-actin was used as a housekeeping gene to normalize the deviations in the p53 gene expression, and the results were related to its mean critical threshold (CT) values by the ΔCT method.

2.6. Immunohistochemical determination of Bcl2 protein

Hela cells treated with the quercetin–based-rhodium(III) complex, for 48 h, were harvested and centrifuged in cooling centrifuges at 1700 rpm for 10 min. The supernatant was aspirated carefully and the cell pellets were washed 3 times with sterile PBS. A volume of 50 µl of treated/untreated cells was aspirated carefully, spread on clean, positive-charged glass slides, and reserved overnight in a cold place. After incubation, all slides were fixed in methanol for 30 min. After fixation, the slides were immersed in primary anti-*Bcl2* antibody for 60 min at 24 °C. Then the slides were dipped in PBS three times, and a suitable amount of the anti-mouse IgG secondary antibody (EnVision + System HRP; Dako) was added and kept for half an hour at 24 °C. The di-aminobenzidine (Liquid DAB + Substrate Chromogen System; Dako) commercial kit was used in visualization of the stained protein. Then, the Mayer's haematoxylin was used as counterstain. Later, the slides were examined with a light microscope. The BCl_2 protein was quantified by calculation of positive cells in no less than 10 high power fields from 1000 cells.

2.7. Protein expression of MMP9 and caspase 9 by western blot analysis

To detect the existence of MMP9 and *caspase 9* proteins, the treated/untreated Hela cell lysed samples were running in SDS gel electrophoresis. After electrophoresis, each protein will be relocated on polyvinylidene fluoride (PVDF) membranes (BioRad) then blocked with 5% nonfat dry milk. To image the MMP9 and *caspase 9* protein, specific primary antibody and anti-β-actin antibody will attached to each protein making a protein-antibody complex. After that, a secondary antibody (EnVision + System HRP; Dako), conjugated with a specific enzyme, was added to be attached to that complex. Then, the enzyme substrate chemiluminescent Western ECL substrate was added to generates luminescence captured by CCD camera-based imager (Chemi Doc imager, Biorad, USA), and the bands intensities were then measured by Image Lab (Bio-Rad). By measuring the amount of luminescence, the quantity of the protein that reacted with the antibody can be calculated.

3. Results and discussion

3.1. General

Quercetin (3,3′,4′,5,7-pentahydroxylflavone) is the common name for the ligand used in the current study and is a natural product of plant origin. Its basic structure is shown in Fig. 1 indicating the polynuclear and polyphenolic features.

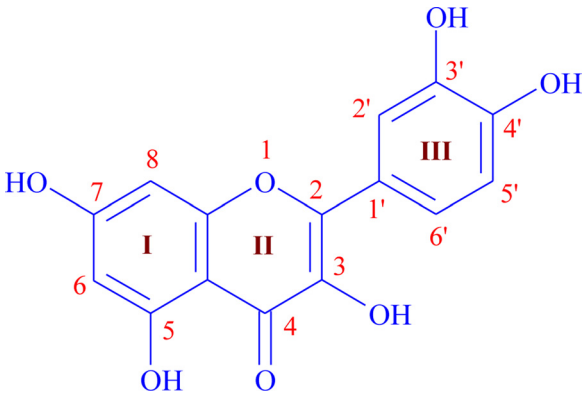

Fig. 1. Quercetin (3,3′,4′,5,7-pentahydroxylflavone) structure.

There are five OH groups in the positions 3,3′,4′,5,7 in addition to a C=O group adjacent to each of the two hydroxyl groups 3 and 5. These structural features allowed quercetin to form metal chelates with many transition metal ions such as ruthenium, copper, iron, cobalt, nickel, zinc, Cd and others [30,41–45]. However, several stoichiometric ratios have been reported, ranging from 1:1, 1:2, 2:1 to 3:1 for the ratio of quercetin to metal ion in the case of Cd^{II}, Cu^{II}, Fe^{II} and rare earth metals respectively [43–46].

For the current quercetin - based Rh(III) complex the analytical results as well as that of TGA showed that the molar ratio is 2:1 (quercetin: Rh^{III}). The molecular formula of the pure isolated Rh^{III} - based quercetin complex is [$RhL_2Cl\ H_2O$]. This complex shows appreciable solubility in water, DMF and DMSO and partial solubility in alcohols such as methanol and ethanol. Electrical conductivity measurements in DMF solution (Table 1) demonstrated the non-electrolytic behavior of the newly synthesized quercetin - based Rh(III) complex [47]. This finding confirms the suggested molecular formula (Table 1) and indicates the participation of the chloride ion as anionic ligand, in the coordination chromophore around Rh(III) ion.

3.2. Thermal analysis

Thermal analysis is one of the techniques that support the results of elemental analysis and help determine the nature of the hydration content accompanying the metal complex molecule. Therefore, thermogravimetric analysis of the rhodium complex under study was conducted to identify the nature of the water content and thermal behavior of Rh^{III} - based quercetin complex. The thermogram of the current metal complex shows three phases of the thermal decompositions (Supplementary materials S2).

The first phase occurs between 190 and 280 °C in several overlapping steps and accompanied by a mass loss of 18.45% with DTG_{max} peaks at 200 °C. The observed mass loss is in an agreement with the theoretical value that corresponds to the volatilization of the coordinated water molecule and chloride anion in addition to the partial decomposition of the organic content. Since the mass loss at this initial stage begins at a temperature of about 200 °C, the surface nature of the water content must be excluded and this finding confirms the coordination bonding of the water molecule.

Table 1
Molecular formula, physical properties and analytical data of quercetin - based Rh(III) complex.

Complex	Color	$\Lambda_{M(}\Omega^{-1}\ cm^2\ mol^{-1})$	Found (calcd.)		
			%C	%H	%M
[$RhL_2\ Cl\ H_2O$]	Dark red	15.22	47.45 (47.59)	2.55 (2.64)	13.76 (13.60)

Table 2
Thermal degradation of quercetin - based Rh^{III} complex [RhL_2 Cl H_2O].

Complex	Temperature °C	DTG_{max} °C	% Mass loss Found (calcd.)	Species formed
[RhL_2 Cl H_2O]	190 – 280	200	18.45(19.37)	[$RhL_{(2-0.17\%)}$]
	280 –485	380, 450	25.25(26.19)	[$RhL_{(2-0.35\%)}$]
	485 – 700	530	40.73(39.75)	Rh_2O_3

Table 3
Infrared spectra (cm^{-1}) of quercetin and its Rh^{III} complex.

Compound	υ(OH)	υ(C = O)	υ(C = C)	υ(C-O-H)	υ(C-O-C)	υ(Rh-O)	υ(Rh-Cl)
Quercetin	3408	1664	1595	1410	1210	–	–
[RhL_2Cl H_2O].	3400	1620	1585	1390	1220	505	380

The second stage of pyrolysis begins at 280, and ends at 485 °C, with DTG_{max} peaks at 380 and 450 °C, indicating mass loss corresponding to the continuous volatilization of the organic content. At this stage, both theoretical and practical values of mass loss agree in explaining the nature of the volatile part of the organic content, as is clear from the results in Table 2.

This thermal decomposition event ends with the third and final stage, which sees the volatilization of the remaining portion of the organic ligand, leaving behind the metal oxide. The brown color of the residual indicates the trivalent state of rhodium in its oxide Rh_2O_3 and not the tetravalent state of rhodium in the black oxide, RhO_2 [48]. This interpretation is based on the remarkable agreement between the theoretical and experimental values (Table 2) of the percentage of metal oxide remaining at the end of the pyrolysis process.

It should be noted that the value of the rhodium content in the remaining oxide (Rh_2O_3) matches the value estimated by the elemental analysis of the suggested formula [RhL_2Cl H_2O].

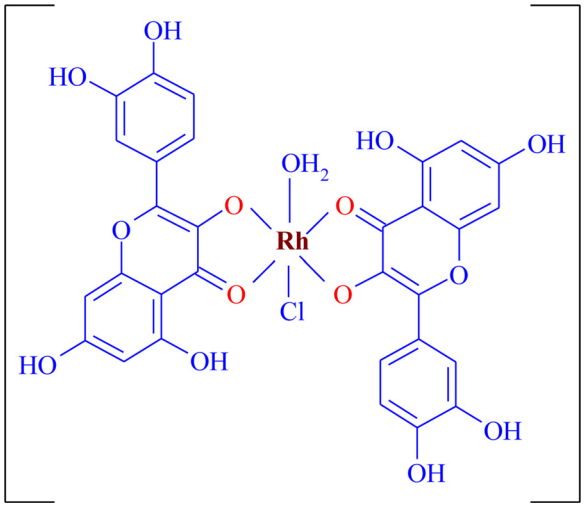

Fig. 2. The proposed structure of quercetin – based Rh(III) complex.

3.3. Verification of the coordination sites and bonding pattern

To verify the coordination sites and bonding pattern of the current metal complex molecule, the infrared spectra of both the free quercetin and its rhodium(III) complex were measured and the related charts are given in S3. In this respect, it is necessary to identify the functional groups in the ligand molecule that are expected to participate in the binding to the metal ion or to be affected by the formation of the metal complex. In this context, the values of the wavenumbers characteristic of the vibrations of these functional groups in both the free quercetin and its metal complex were determined as mentioned in Table 3. The data in Table 3, revealed that the characteristic stretching of the carbonyl group, υ(C = O), for the free quercetin appears at 1664 cm^{-1} was shifted to lower wavenumber, 1620 cm^{-1}, in the spectrum of the metal complex. This finding indicates involvement of the carbonyl oxygen in coordination to Rh^{III} ion [49].

The question now is which of the hydroxyl groups, 3 or 5, adjacent to the carbonyl oxygen will participate in the bonding to the metal ion. Since the bonding of the metal ion to the hydroxyl oxygen takes place with the deprotonated hydroxyl oxygen, so the acidity of the OH group will determine the hydroxyl group that participates in the bonding to the metal ion. Referring to the structure of the quercetin molecule (Fig. 1), we find that the hydroxyl group on site 3 is more acidic than that on site 5. This is due to the fact that, the hydroxyl group on site 3 is closer to the oxygen of the carbonyl group than the hydroxyl group on position 5. In addition, the ring to which the hydroxyl group is attached to the position 3 is heterogeneous due to the presence of the highly electronegative oxygen atom. These structural features of the quercetin molecules in turn increase the degree of acidity of OH in position 3 over OH in position 5. However, previous relevant studies support an OH at position 3 above position 5 in the formation of quercetin metal complexes [42,43,50]. This finding is supported by the observed decrease in the bond order of the two oxygen atoms groups, C=O and OH on site 3 due to coordination to the metal ion in the metal chelate which may give rise to a coupling of stretching of these two bonds. In the same context, the spectrum of the Rh^{III} – quercetin based chelate shows two new bands at 1390 and 1440 cm^{-1} which can be considered to be related to the symmetric and asymmetric stretching modes of (C–O) group respectively at the chelation site [43].

The non-participation of ring oxygen in the formation of the metal complex is supported by the slight change in the frequency of both υ(C–O–C) and υ(C=C) of ring **II** (Fig. 1). Alternatively, the new medium band appears at 505 cm^{-1} in the spectrum of quercetin - based Rh^{III} complex is assigned to υ(Rh–O) and confirm complex formation [49]. Participation of the chloro anion (Cl^-) in the coordination chromophore of the newly synthesized rhodium(III) chelate is evidenced from the presence of the characteristic frequency of the bonding of the Rh^{III} ion with the chloride anion υ(Rh – Cl) at 380 cm^{-1} [49]. In the same respect, the presence of coordinated water was inferred from the broad band present at 3400 cm^{-1} in the spectrum of the metal complex that did not appear in the free quercetin spectrum [49]. However, thermogravimetric measurements indicated the coordination nature of the water content in the molecule of the present metal complex.

Based on the aforementioned results and discussions, the structural formula of the present quercetin – based Rh^{III} complex has been proposed as given in Fig. 2.

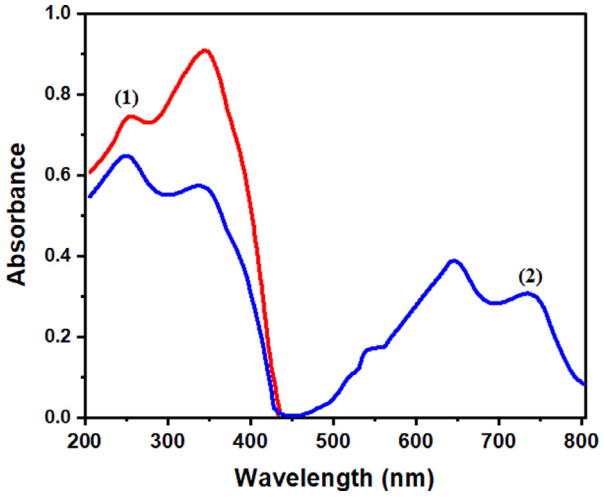

Fig. 3. Electronic absorption spectra of quercetin (1) and quercetin – based Rh^{III} complex (2) in DMF solution at room temperature. (For interpretation of the references to color in this figure legend, the reader is referred to the web version of this article.)

Table 4
Crystallographic data of quercetin – based Rh^{III} complex.

Empirical formula	$C_{32}H_{25}ClRhO_{15}$
Formula weight	787.89
T (K)	305
λ (Å)	1.529040
Crystal system	Monoclinic
Space group	P2/m
Centro symmetry	Acentric
Space Group Number	4
Z	2
Multiplicity	2
Bravais Lattice	P
Lattice Symbol	mP
Unit cell dimensions:	
a (Å), *b* (Å), *c* (Å)	5.881, 9.597, 3.063
α (°), β (°), γ (°)	90.000, 95.122, 90.000
Cell volume (Å^3)	172.161
Volume per atom (Å^3)	1.757
Calculated density (g/cm^3)	5.57
θ range for data collection (°)	30.000 – 80.000
Total reflection	693
Rietveld results:	
Rp	18.726
Rwp	24.381
R-Bragg	1.044
R-F	1.240

3.4. UV–Vis spectral and magnetic investigations

Rhodium(III) belongs to d^6 – transition elements with $^1A_{1g}$ ground state. The hexa- coordinated Rh(III) center in an octahedral configuration, is characterized by the low energy spin–forbidden transition $^1A_{1g} \rightarrow {}^3T_{1g}$ (υ_1) and the two spin – allowed transitions $^1A_{1g} \rightarrow {}^1T_{1g}$, ($\upsilon_2$) and $^1A_{1g} \rightarrow {}^1T_{2g}$, ($\upsilon_3$) in an energy order of $\upsilon_1 < \upsilon_2 < \upsilon_3$ [51,52]. The room temperature spectrum in DMF solution for the present quercetin - based Rh^{III} complex exhibits three absorption bands (Fig. 3) at 740, 645, and 545 nm ascribed to the electronic transitions, υ_1, υ_2 and υ_3, in the octahedral stereochemistry [52,53]. The energies of these electronic transitions are similar to other six-coordinated rhodium(III) complexes in an octahedral geometry [52–56].

To clarify the electronic properties of the studied compounds, the spectra of free quercetin and its Rh(III) chelate were measured under the same conditions and related spectra are given in Fig. 3. In this regard, two strong absorption bands are observed at relatively high-energy positions 255 and 350 nm in the case of uncomplexed quercetin. These bands are associated with the $\pi \rightarrow \pi^*$ aromatic transition of the cinnamoyl and benzoyl systems of the rings **III** and **I** respectively of the quercetin ligand (see Fig. 1). In the spectrum of the quercetin – based Rh(III) complex, the electronic transitions related to the quercetin component appear approximately in the same energy regions as in the case of free quercetin.

Magnetic susceptibility measurements at room temperature demonstrated the diamagnetic character of the magnetically diluted quercetin - based Rh(III) complex. This finding indicates the low-spin state (t_{2g}^6) of the six coordinated Rh(III)-core with d^2sp^3 hybridization in an octahedral stereochemistry.

3.5. PXRD-structural analysis

Nowadays, PXRD results processing technology with specialized computer software, such as Expo 2014, for structural analysis of metal complexes has become an alternative to X-ray structural analysis for a single crystal [36]. In this regard, the Rietveld-Refinement methodology is used to reach a high degree of agreement between the practical results and the computer processing of the X-ray spectroscopic data of the metal complex under study.

Fig. 4 shows the PXRD spectrogram of quercetin – based Rh^{III} complex while Fig. 5 shows the degree of agreement between the practical results and computer calculations.

Table 4 summarizes the relevant crystallographic information of quercetin - based Rh^{III} complex that crystallizes in crystal system monoclinic space group P2/m with cell parameters $a = 5.881$, $b = 9.597$ and $c = 3.063$ Å. It is noticeable that *a, b* and *c* do not correspond exactly *x, y* and *z* because one of the three angles of the monoclinic structure is unequal to 90° (see Table 4).

Fig. 6 illustrates the numbering drawing adopted for the optimized coordination polyhedron in an octahedral configuration and the hydrogen atoms have been omitted for clarity.

The structural diagram in Fig. 6 indicates that the four oxygen atoms O(2), O(7), O(8) and O(9) occupy the Basel plane of the octahedral geometry around Rh^{III}- center. In the same respect, the anionic ligand Cl(1) and the oxygen atom O(10) of the coordinated water molecule are located on the two axial positions. The determination of the type of atoms occupying the vertical axis was based on the value of the bond between these two donor sites Cl(1)-Rh(1)-O(10)= =171.27. This angle has the largest value in comparison to the angles between the opposite sites in the Basel plane O(2)-Rh(1)-O(8)= =170.74 and O(7)- Rh(1)-O(9)= =168.52 (Table 5). Also, the bond distance between Rh(1) and the two axial Cl(1) and O(10) donor sites is longer than that between Rh(1) and the four basal plane donor sites (Table 6). This noticeable elongation of the axial bond distance indicates a tetragonal distortion in the octahedron structure of the current quercetin – based Rh(III) complex.

The packing diagram of the unite cell which includes two molecules of metal complex is illustrated in Fig. 7.

It is known that, metal complexes with coordination number six take the stereoscopic shape of an octahedron. The question arises about the perfection of this stereotype; is it an ideal octahedron or a trigonal prism? The geometric index τ_6 value was estimated from the relationship $\tau_6 = = \theta/60$ and will decide the matter; with note that θ is the torsion angle between opposite trigonometric faces in the octahedron. In the case that the τ_6 is equal to one, this indicates a perfect octahedron, while in the case of the τ_6 equal to zero the related structure is ideal trigonal prism [57,58]. The determined value of τ_6 is 0.95 that confirms the ideal-

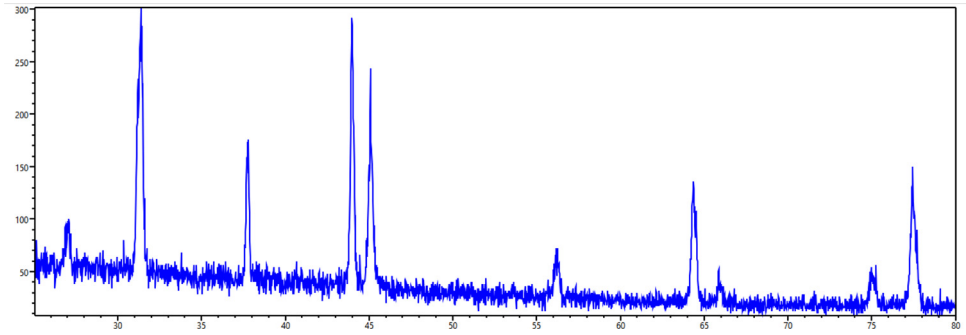

Fig. 4. The microcrystalline XRD spectrum of quercetin – based Rh^{III} complex.

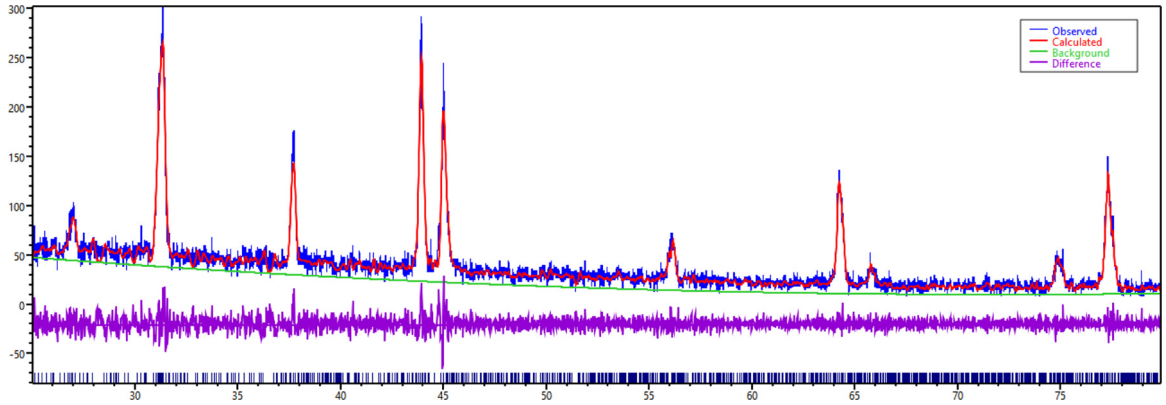

Fig. 5. Good match between the experimental and calculated data for the microcrystalline XRD–spectrum based on Rietveld Refinement for quercetin – based Rh^{III} complex.

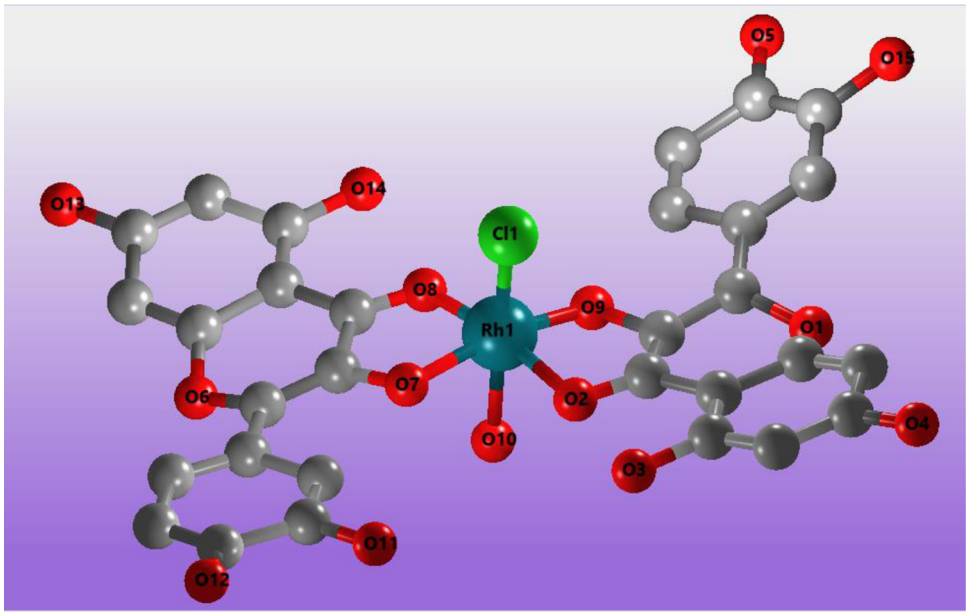

Fig. 6. Structural diagram of the optimum numbering of the octahedral configuration for quercetin - based Rh^{III} complex.

ity of the octahedral structure of the current quercetin–based Rh^{III} complex.

3.6. Biomimicking SOD catalytic activity

The SOD like activity of present quercetin–based Rh^{III} complex was evaluated spectrophotometrically by determining the percentage change in the optical density produced from the reduction of NBT to formazan (F) due to the presence of the metal complex. In this assay, phenazine methosulphate (PMS) is a light-induced $O_2^{\bullet-}$ production source that reacts with NBT to form formazan as described in reaction 1:

$$NBT + O_2^{\bullet-} \xrightarrow{k} (F) \quad (1)$$

The rate of formazan formation is defined in relationship 2:

$$d[F]_1/dt = k[NBT][O_2^{\bullet-}] \quad (2)$$

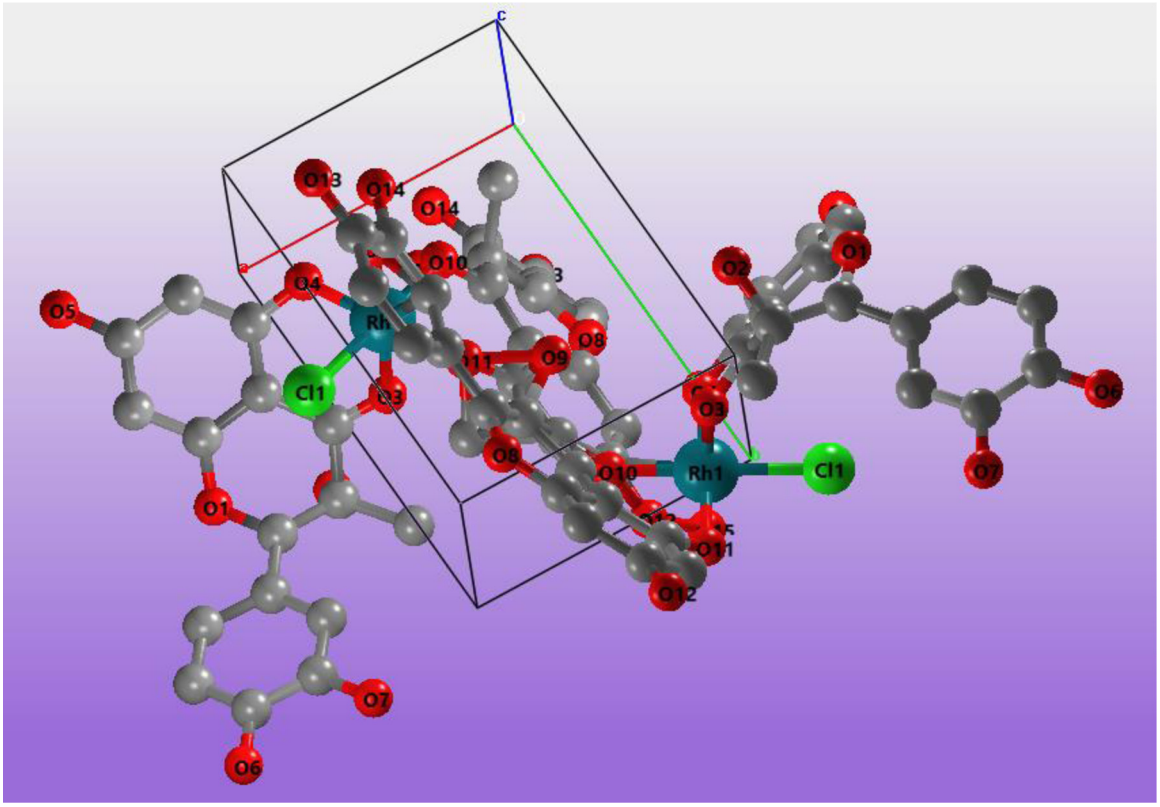

Fig. 7. Stereo view of the packing diagram of the unite cell which includes two molecules of metal complex.

Table 5
The relevant bond angle (°) around Rh(III) – core of [$Rh^{III}L_2Cl\ H_2O$].

(θ= 57); Octahedral τ_6=0.95	
O2-Rh1-O7	86.39
O2-Rh1-O8	170.74
O2-Rh1-O9	86.54
O2-Rh1-Cl1	88.91
O2-Rh1-O10	83.84
O7-Rh1-O8	87.67
O7- Rh1-O9	168.52
O7-Rh1-Cl1	92.04
O7- Rh1-O10	82.69
O8-Rh1-O9	98.15
O8-Rh1-Cl1	98.4
O8-Rh1-O10	88.36
O9-Rh1-Cl1	96.86
O9-Rh1-O10	87.57
Cl1-Rh1-O10	171.27

Table 6
The relevant bond distances around Rh(III) – core of [$Rh^{III}L_2Cl\ H_2O$].

Bond type	Bond distance (Å)
Rh1 - O2	2.043
Rh1 - O7	2.025
Rh1- O8	1.807
Rh1 - O9	1.849
Rh1 - Cl1	2.104
Rh1 - O10	2.065

The native SOD protein catalyzes disproportionation of $O_2^{\bullet-}$ as shown in Eq. (3):

$$M^{n+} - SOD + O_2^{\bullet-} \xrightarrow[2H^+]{k_c} M^{n+} - SOD + H_2O_2 + O_2 \quad (3)$$

In the same way, question–based Rh^{III} complex will act as the native M^{n+}-SOD and the inhibitory rate of formazan development after adding the current Rh^{III} complex is assumed from the Eq. (4):

$$d[F]_2/dt = k_c[Rh^{III}\ complex][O_2^{\bullet-}] \quad (4)$$

The catalytic rate constant k_c (second order) is defined as shown in the relationship 5:

$$d[F]_1/\ d[F]_2 = \Delta_1/\Delta_2 = 1 + k_c[Rh^{III}\ complex]/\ k[NBT] \quad (5)$$

where Δ_1 and Δ_2 are the relevant optical density at 560 nm in the absence and in the presence of the Rh^{III} complex respectively.

The concentration of the quercetin–based Rh^{III} complex (IC_{50}) at which NBT reduction is inhibited by 50% was determined graphically (Fig. 8) with knowing that NBT%= $=(\Delta_1/\Delta_1 - \Delta_2) \times 100$.

Since the IC_{50} α [NBT], thus $k_c = k$[NBT]/IC_{50}; where k, is $5.94 \times 10^4\ M^{-1}\ s^{-1}$ and [NBT] is 30 μM [58].

The estimated values of IC_{50} and k_c are 21.9 μM and $8.91 \times 10^4\ M^{-1}\ s^{-1}$ respectively indicating that the SOD mimetic catalytic activity of the quercetin – based Rh^{III} complex is somewhat moderate and similar to related low-spin d^6 metal complex (Table 7).

The mid value of the catalytic activity of the rhodium(III) complex in question could be ascribed to structural reasons. In this regard, the catalytic dismutation of $O_2^{\bullet-}$ will begin after the bonding of the superoxide anion radical to the Rh^{III} center. Therefore, the spark of the catalytic cycle is the easy exchange of $O_2^{\bullet-}$ with one of the six coordination sites of the octahedral structure. Although the complex molecule in question is coordinately saturated and does not have empty coordination sites for binding $O_2^{\bullet-}$ but it has two well-departing groups namely H_2O and Cl. In this con-

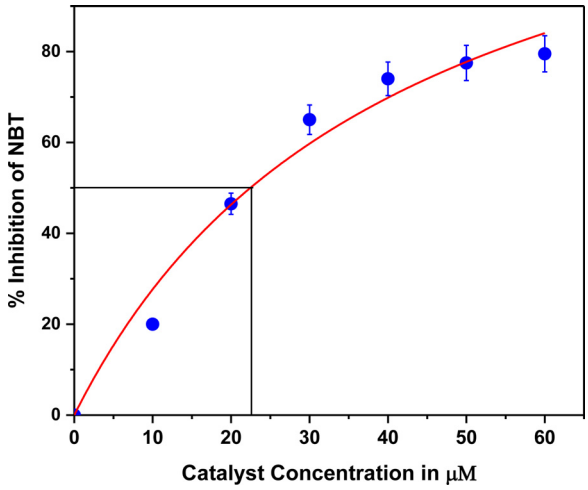

Fig. 8. Scheme of percentage reduction of NBT inhibition with increasing the concentration of quercetin-based Rh^{III} complex.

Table 7
Comparison the biomimetic SOD activity of quercetin – based Rh^{III} complex with others SOD mimics.

Complex	IC_{50} (μM)	k_c (M^{-1} s^{-1})	Reference
$[Rh^{III}L_2Cl\ H_2O]$	21.9	8.91×10^4	This work
$[(CoL_2)_2O_2Cl_2]Cl_2\ 2H_2O$	31.0	5.75×10^4	[36]
$[CoL^XL^Y]Cl$	87.0	3.82×10^4	[59]
$[Fe^{III}L_2Cl_2]Cl\ H_2O$	17.0	1.05×10^5	[36]
Fe^{III}TPAA	7.5	7.92×10^5	[60]
$[(Mn^{III}L_2)_2O_2Cl_2]Cl_2\ 2H_2O$	8.0	22.2×10^5	[36]
$[MnL^8]$	0.77	3.6×10^6	[58]
$[MnL^9]$	1.14	2.4×10^6	[58]
$[MnL^{10}]$	2.34	1.2×10^6	[58]
MnSOD and FeSOD*	–	$\sim 10^9$	[61]

* Indicated native enzymes.

text, the labile potency of the existing metal complex is the key that tuning its catalytic potential.

According to Taube, the degree of liability or inertness of a transition metal complex can be correlated with the *D*-electronic configuration of the metal ion [48]. For the octahedral structure, if a complex contains electrons in the anti-bonding orbitals e_g^*, the ligands are expected to be relatively weakly bound and easily displaced; it is labile, while for a complex with empty e_g^* it is inert [48]. In the same context, if all the three- t_{2g} levels are filled either singly or doubly, then the complex is inert kinetically. In any case, when it comes to the reactivity of complexes, the phrases "labile" and "inert" are simply comparable. In general, complexes of (0.1 M) should be termed labile if they entirely react in less than one minute, and inert if they take longer.

However, the electronic configuration of the present Rh^{III} center in the low-spin octahedral geometry is $t_{2g}^6e_g^0$ and thus it is kinetically inert and this may explain its mid catalytic potential.

Several studies concluded that the natural enzyme always remains the highest in activity compared to its functional models listed in Table 7 as well as mentioned in the literature.

3.7. Proposed catalytic mechanism

All previous studies demonstrated that the catalytic dismutation of $O_2^{\bullet-}$ by the M-SOD protein [61] or the SOD-mimics occurs in a ping pong pattern [36,37,58]. Likewise the current quercetin-based Rh^{III} complex catalyzes the dismutation of $O_2^{\bullet-}$ in a ping-pong mechanism. In this regard, initiation the catalytic cycle begins with the exchange of bonding between $O_2^{\bullet-}$ and the anionic ligand (Cl^-) which leads to binding of $O_2^{\bullet-}$ to rhodium(III) center to form the intermediate $[(O_2^{\bullet-})\text{-}Rh^{III}L_2H_2O]$. Electron transfer from $O_2^{\bullet-}$ to Rh^{III} center follows this step which results in the reduction of Rh^{III} to Rh^{II} with release of a molecular oxygen molecule (O_2). The second redox reaction occurs due to binding of the second $O_2^{\bullet-}$ to Rh^{II} center with spontaneous oxidation of Rh^{II} to Rh^{III} and reduction of $O_2^{\bullet-}$ to O_2^{2-}. Protonation of O_2^{2-} before releasing is essential due to the high basicity of O_2^{2-}. Therefore, in successive steps, O_2^{2-} is protonated and liberated as H_2O_2 and the catalyst returns to its primary form as shown in Scheme 1.

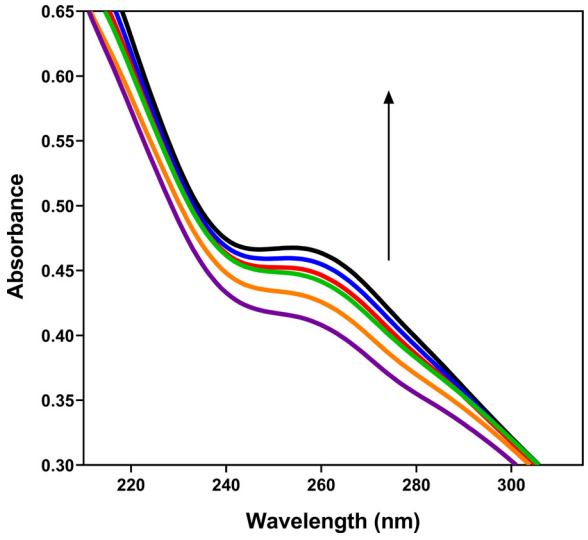

Fig. 9. Absorption spectra of quercetin-based Rh^{III} complex (15 μM) in lack and existence of increasing amounts of CT-DNA (2 - 12 μM) in Tris–HCl buffer (pH = 7.2).

3.8. DNA binding study

The interaction between DNA and metal complexes is commonly studied using electronic absorption spectroscopy. The DNA binding capacity of the current querectin–based Rh(III) complex with calf thymus (CT)-DNA was evaluated by monitoring the spectroscopic changes of the electronic spectra of CT-DNA due to the interaction with the metal complex. However, interaction of CT-DNA with the metal complex leads to spectral changes which, by their characteristics, can determine the mode of interaction between the metal complex and DNA. For example, at a fixed concentration of a metal complex and a sequential rise in the concentration of CT-DNA, the spectral change was detected leading to hyperchromism or hyporchromism that may be associated with red shift or blue shift [62]. Hyporchromism indicates the intercalation mode, while hyperchromism occurs when the external contact pattern (groove/electrostatic binding) is dominant [63,64].

For the current study, an absorbance titration experiment was performed using a fixed concentration of quercetin-based Rh(III) complex to which increments of CT-DNA stock solution were added and the obtained results are represented in Fig. 9.

As shown in Fig. 9, the spectral changes for the quercetin-based Rh^{III} complex at 250 nm due to π-π^* intra-ligand transition showed an increase in absorbance (hyperchromism) with a noticeable red shift of about 4 nm, indicating the stability of the DNA helix. This result indicated a surface binding to DNA [65,66], which leads to damage to the secondary structure of CT-DNA, as the phosphate group can provide the appropriate anchors to coordinate with the metal complex [67,68]. A similar behavior of such kind of interaction of DNA with quercetin-iron has been already reported [43].

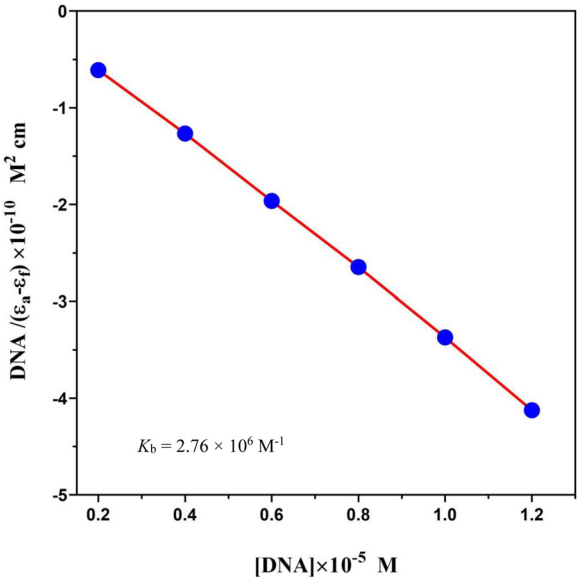

Fig. 10. Plot of [DNA]/(ε_a-ε_f) *versus* [DNA] for the DNA binding assay of quercetin – based Rh(III) complex. [DNA] is the concentration of CT-DNA in base pairs, ε_a corresponds to the extinction coefficient observed (A_{obs}/[complex]). ε_f is the extinction coefficient of the free complex, ε_b is extinction coefficient of the complex fully bound to CT-DNA, and k_b is the intrinsic binding constant.

In the same context, the intrinsic binding constants, K_b, of the complex was determined using the following equation [67]:

$$\frac{[DNA]}{(\varepsilon_{a-}\varepsilon_f)} = \frac{[DNA]}{(\varepsilon_{b-}\varepsilon_f)} + \frac{1}{k_b(\varepsilon_{b-}\varepsilon_f)} \quad (5)$$

The ratio of slope to intercept in the plot of [DNA]/(ε_a-ε_f) *versus* [DNA] (Fig. 10) gave the value of K_b. The calculated K_b value of the quercetin-based Rh^{III} complex was found to be 2.76×10^6 M^{-1} which can be compared with the analogous quercetin-based ruthenium complex with a K_b value of 3.05×10^3 M^{-1} [41,69]. Since quercetin is the common ligand for both ruthenium(III) and rhodium(III) complexes, the marked variance in the binding ability with DNA is due to the type of metal ion. In the same context, the value of the intrinsic binding constant, K_b, of the quercetin-based Rh(III) complex is much higher than that of the quercetin-based Ru(III) complex and this finding indicates that the Rh(III) quercetin-based complex is relatively tightly bound to the DNA.

3.9. DPPH scavenging power

To confirm the scavenging power of the rhodium(III) complex under study to remove free radicals, an additional test of its ability for scavenging DPPH was performed. The ability of a compound to neutralize a free radical is measured by DPPH's scavenging activity by forming a bond with the radical, resulting in an inert product, or by providing hydrogen to the free radical. To measure that activity, the compound was reacted with the DPPH solution and the disappearance of the DPPH color was related to its scavenging activity [70]. Our data revealed a significant decrease ($p = 0.047$) in the DPPH IC_{50} value of the quercetin – based Rh^{III} (23.53 ± 3.56) compared with the DPPH IC_{50} value of the quercetin (36.99 ± 3.13), which established the increased ROS scavenger power of the quercetin – based Rh^{III} than the free quercetin (Fig. 11). This superiority in the antioxidant activity of the examined rhodium(III) complex can be attributed to cooperative action between the rhodium(III) center and the two coordinated quercetin compartments of whole metal chelate molecule.

From that we can conclude that, the results obtained from the DPPH scavenging activity assay are consistent with the results of the SOD-mimicking catalytic activity of the polyphenolic natural product quercetin and its rhodium(III) compound.

Table 8
Mean IC_{50} values (± SEM) of quercetin and its Rh^{III} complex against different cancer human cell lines as well as normal cell line (WI38) compared with cisplatin.

Compounds	Quercetin	Quercetin – based Rh^{III}	Cisplatin
HepG-2	129.28 ± 13.5*#	8.49 ± 0.4#	4.50 ± 0.12
Hela	68.78 ± 1.39*#	9.40 ± 0.46#	5.57 ± 0.23
MCF-7	61.72 ± 3.29*#	16.32 ± 0.81#	4.17 ± 0.12
PC-3	91.92 ± 7.32*#	17.71± 0.87#	8.87 ± 0.635
Caco-2	80.92 ± 9.04*#	21.73 ± 1.13#	12.49 ± 0.64
WI38	454.5 ± 48.1*#	40.58 ± 2.8#	6.72 ± 0.29

* $p < 0.05$ significant compared with the quercetin – based Rh^{III} complex.
# $p < 0.05$ significant compared with cisplatin.

3.10. In vitro cytotoxic activity

The cytotoxic effect of both quercetin and its rhodium(III) complex were determined, in triplicated manner, against HepG-2, Hela, MCF-7, PC-3, Caco-2 and WI38 as a normal cell line. Cisplatin was used as standard anticancer drug in all cell lines. A concentration scale from 100 to 1.56 μg/ml of quercetin and its rhodium(III) complex and cisplatin were freshly prepared and every dilution was added into a well cultured with 0.5×10^5 cells, then incubated for 48 h. The cytotoxic effects of both quercetin and its rhodium(III) complex were assessed by MTT assay and the IC_{50s} were calculated and compared with cisplatin IC_{50}.

Fig. 12 presents different human cancer cells viabilities (%) that regularly reduced with increasing the quercetin – based Rh^{III} complex concentration which proven the anti-proliferative effect of that complex in a concentration dependent manner. The IC_{50} values of the quercetin – based Rh^{III} against the five cell lines were significantly reduced compared with uncomplexed quercetin ($p \leq 0.0001$, for all, Table 8) confirming the improved anticancer activity of the quercetin – based Rh^{III} complex. Also, the IC_{50} values of quercetin – based Rh^{III} complex were approximately two folds increased on HePG-2, Hela and PC-3 cells compared with cisplatin indicating potent anticancer activities of the current Rh(III) complex against those cell lines. Alternatively, the IC_{50} of quercetin – based Rh^{III} complex against the normal cell line (WI38) was significantly increased compared with cisplatin indicating reduced toxicity to normal cell. These data indicated the efficient anti-proliferative activities of the quercetin – based Rh^{III} complex compared with standard anticancer agent (cisplatin) with increased safety on normal cells.

3.11. Quercetin – based Rh^{III} complex apoptotic effect on Hela cell

The percentages of apoptosis and necrosis were quantitatively assessed in the Hela cells after treatment with quercetin – based Rh^{III} complex by the Annexin V/PI stain. Normal cells were designed for apoptotic cell death, but malignant cells had inhibited that route. In apoptosis, nucleus fragmentation appears then the cell was shrank stimulating the phagocytic cell to engulf it [71]. While, in necrosis the dysfunction of the plasma membrane appeared leading to cell swelling then suddenly exploded causing inflammation in a wide area [72]. Fig. 13 shows a significant increase in the total apoptotic cell death (%) as sum of early and late apoptosis in the Hela cells treated with the IC_{50} of the synthesized Rh^{III} complex compared with untreated Hela cells ($p \leq 0.0001$). These results proposed that the quercetin – based Rh^{III} complex may inhibit the Hela cells proliferation through induction of apoptosis (Fig. 13C). To endorse the hypothesis of apoptotic pathway; the cell

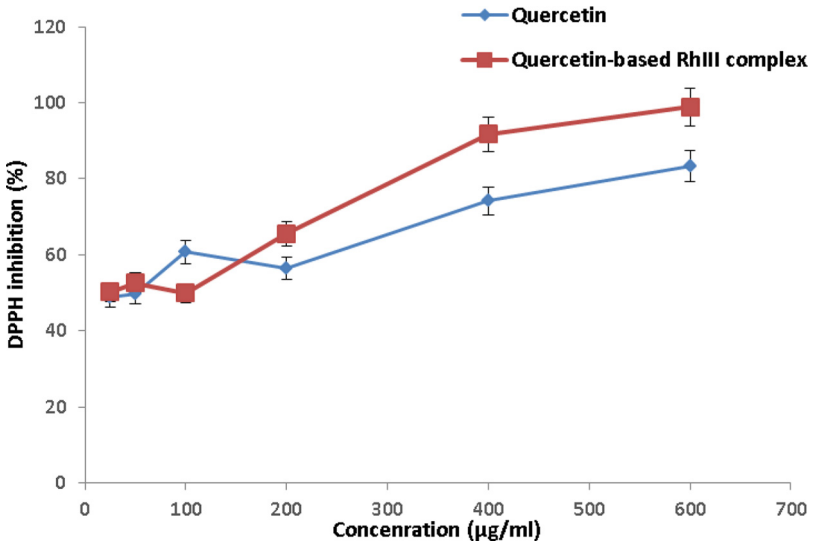

Fig. 11. DPPH inhibition percentage curve of quercetin – based Rh^{III} complex and free quercetin.

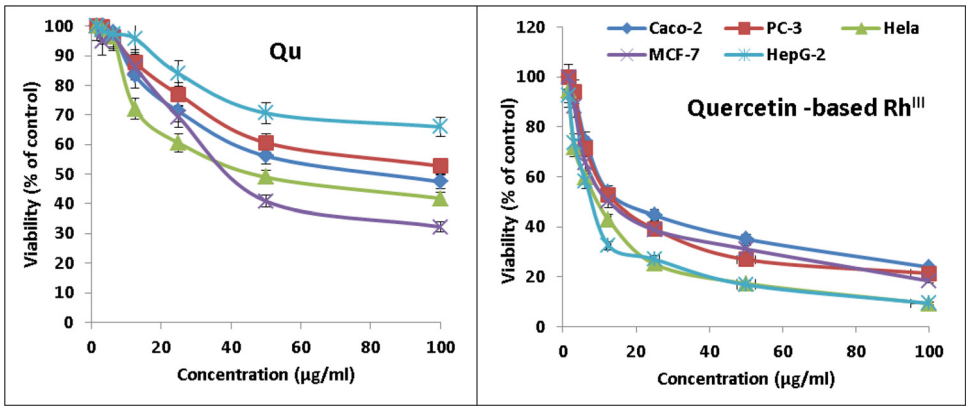

Fig. 12. Viability percentage of the human cancer cell lines after treatment with quercetin (Qu) or quercetin – based Rh^{III} complex.

cycle was assessed on the Hela cells treated with quercetin – based Rh^{III} complex.

3.12. Cell cycle arrest prompted by quercetin – based Rh^{III} complex

Division of the cells at certain phases in order to replicate is called cell cycle. G1 (Gap 1) is the first phase to trigger the cell cycle, then S and G2 phases and ends with mitosis (M phase). The Hela cells were treated with the IC_{50} of the quercetin – based Rh^{III} complex and incubated for 48 h, then the cell cycle was estimated by flow cytometer using PI. The average percentage of cells in each phase was calculated. The propagation in cell count (%) in the pre-G1 phase was associated with late apoptotic death of malignant cells [73]. The arrest in the pre-G1 phase could be attributed to prevention of DNA replication, stopping cell multiplication, leading to a decrease in G2/M phase [39].

As shown in Fig. 13, the Hela cells treated with the present Rh^{III} complex were arrested in the pre-G1 phase as a huge propagation of cells was detected compared with untreated Hela cells ($p \leq 0.0001$). On the other hand, a significant decrease in G2/M percentage was observed in Hela cells treated with the quercetin – based Rh^{III} complex compared with untreated cells ($p = 0.025$). That amplification in pre-G1 cell count indicated that the quercetin – based Rh^{III} complex has prevented malignant cells from entering another cell cycle by surface binding with DNA to avoid its replication (Fig. 13D), as observed from the DNA binding study. By inhibiting DNA replication, the cell cycle stopped, and mitosis decreased, as observed in the depletion of G2/M percentage. To prove the apoptotic pathway of the quercetin – based Rh^{III} complex on Hela cells, the p53, MMP9 and caspase 9 gene expressions were detected and compared with untreated cells.

3.13. Quercetin – based Rh^{III} complex effect on p53 genes and Bcl2 protein

P53 is a protein that, when activated, can suppress any mutation that happens in cells, so it is known as a tumor suppressor gene. To suppress mutation, p53 can promote cell cycle arrest, inhibit DNA damage, and initiate apoptosis for malignant cells [74,75]. Cancer cells could diminish p53 gene activity to proliferate abnormally [76–78]. The current data indicated a markedly significant upregulation of p53 gene expression ($p \leq 0.0001$) in the Hela cells treated with quercetin – based Rh^{III} complex compared with untreated cells (Fig. 13A). P53 gene upregulation demonstrated that the quercetin – based Rh^{III} complex may stop Hela cells proliferation through the p53 pathway. These data are complementary

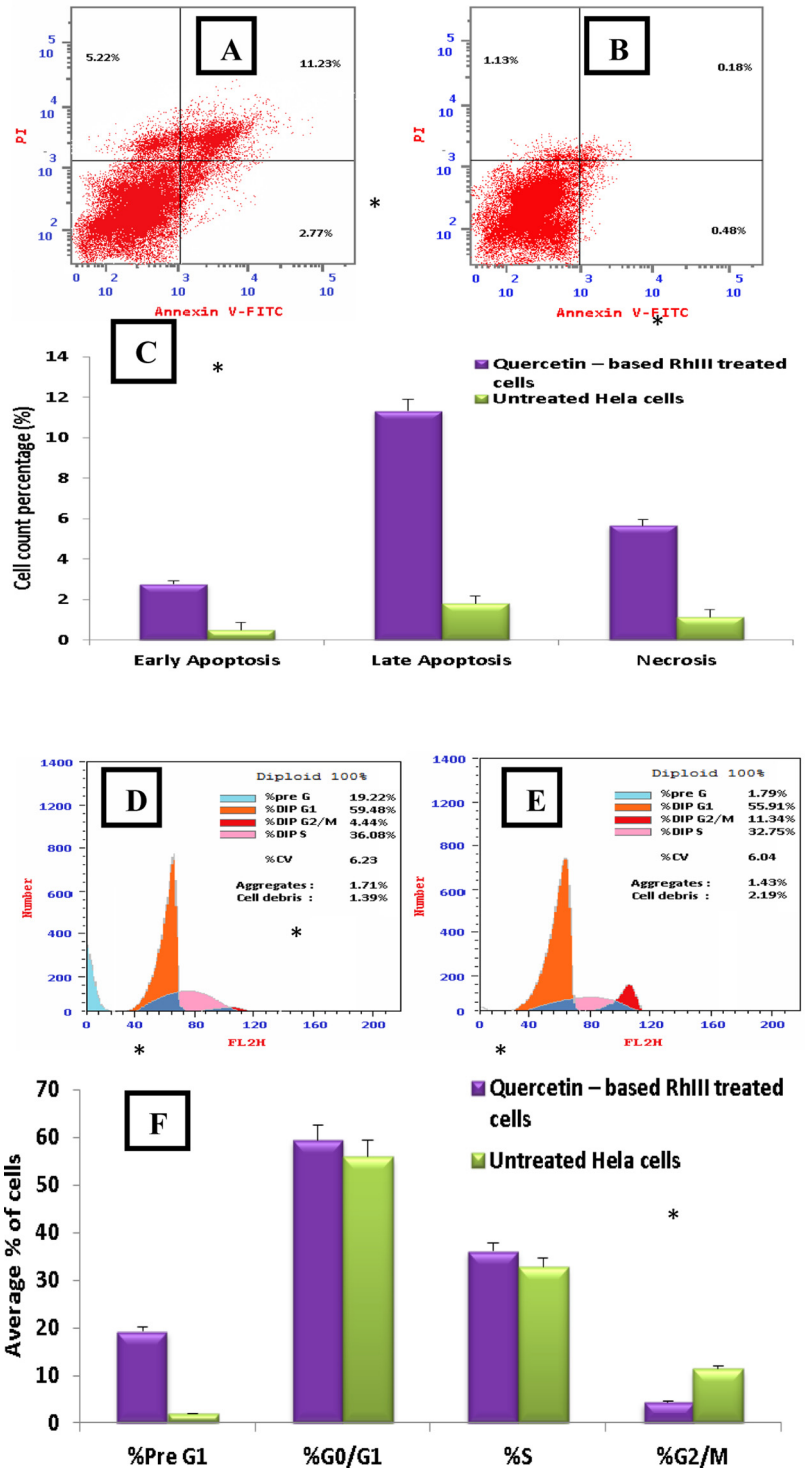

Fig. 13. The apoptotic/necrotic percentage in Hela cell treated with quercetin – based Rh^{III} complex compared with untreated cells (A&B). Bar plots represented early, late apoptosis and necrosis percentage (C). The cell cycle distribution in Hela cell treated with quercetin – based Rh^{III} complex compared with untreated cells (D&E). Bar plots represented cell cycle distribution (%) (F) * $p < 0.05$ significant compared with untreated cells.

to our former results that the quercetin – based Rh^{III} complex can induce Hela cells apoptosis and reduce mitosis in the G2/M phase via the p53activation.

Bcl2 (B-cell lymphoma 2) is a protein that plays an essential role in cancer progression by shutting down apoptosis [79,80]. Recently, innovative chemotherapeutic agents have been planned to inhibit *Bcl2* activity [81]. Also, the up-regulated p53 gene can inhibit *Bcl2* protein and trigger apoptotic cell death in cancer cells [82].

Our immunohistochemistry data revealed a significant decrease ($p \leq 0.0001$) in the *Bcl2* protein in the Hela cells treated with the quercetin – based Rh^{III} complex compared with untreated cells (Fig. 14B & C). That decrease in the *Bcl2* protein could be evidence of the apoptotic pathway through activating p53.

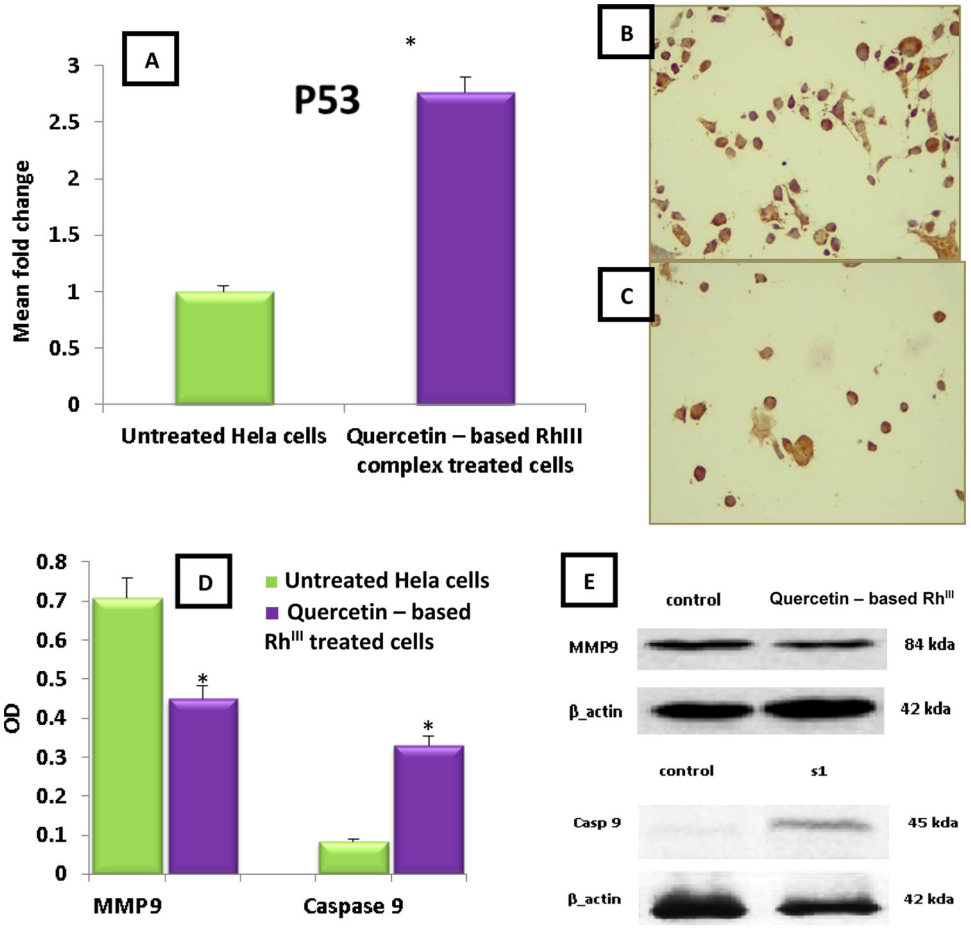

Fig. 14. Bar plots presentation of RT-PCR analysis of the mean fold change of the p53 (A). Immunohistochemical analysis of *Bcl2* gene in Hela cells treated with quercetin – based Rh^{III} complex (C) compared with untreated cells (B). Bar plots and representative western blot of MMP9 and caspase 9 gene expression levels in Hela cells treated with IC_{50} of quercetin – based Rh^{III} compared with untreated cells (D&E). β-actin was considered as standard gene control. $^{*}P < 0.05$ significant compared with untreated Hela cells.

3.14. Quercetin – based Rh^{III} complex influence on MMP9 and caspase 9 proteins

MMP9 is one of the matrix metalloproteinases that can denature extracellular matrix components, leading to cell membrane destruction. That destruction promoted malignant cell metastasis [83]. High levels of MMP9 were noticed in different types of cancers [84–87].

Caspases are protelytic enzymes that will be triggered at the end-stage of apoptosis to cleavage the DNA and split the cell membrane of the mutated cells [88]. Apoptotic cell death could be identified by the activation of the caspases. Extrinsic and intrinsic apoptotic signaling pathways are the principal cell death pathways [89]. Both pathways end with caspase 8, 9 or 10 activation, triggering the caspase3 cleavage [90,91]. Caspase3 consequantly degrades DNA, split the membrane component and promotes the apoptotic death [92].

Our western blot image presented a significant decreased level of MMP9 protein ($p = 0.026$) with a significant increase in caspase 9 level ($p = 0.009$) in the Hela cells treated with the quercetin – based Rh^{III} complex compared with untreated cells (Fig 14D&E). The decline in MMP9 level has proven the anti-proleferative and anti-metastasis effects of the quercetin – based Rh^{III} complex against Hela cells.

From our former data, we can hypothesize that the quercetin – based Rh^{III} complex anti-proliferative effect is by binding to the DNA surface which prevent cancer cell replication with increasing the p53 levels. Increased p53 can inhibit both *Bcl2* and MMP9, then activating caspase 9, which then cleaves caspase 3, leading to apoptosis triggering. Apoptosis activation led to cell cycle arrest at the pre-G1 phase and decreased Hela cell proliferation, which appeared in the decreased G2/M phase.

3.15. Antioxidant activity of the quercetin – based Rh^{III} complex

High cancer cells' proliferation is always accompanied with high metabolic activities. High metabolic activities led to excess reactive oxygen species (ROS) [93]. Excess ROS have important role in cancer proliferation by starting DNA damage and controlling metabolism [94]. In normal cells, the antioxidant system is there to consume the ROS produced by metabolism. From these antioxidant enzymes is the superoxide dismutase (SOD), which removes the superoxide radicals by converting them to H_2O_2 [95,96]. Stimulation of high SOD production can lead to apoptotic cell death in malignant cells [97].

The DPPH assay improved the high scavenging activity of the quercetin – based Rh^{III} complex with its high *in vitro* SOD like activity. To confirm the antioxidant activity inside cancer cells, the SOD activity was evaluated in Hela cells treated with the quercetin – based Rh^{III} complex compared with untreated cells. Our data revealed a markedly significant increase in the SOD activity in Hela cells treated with quercetin – based Rh^{III} complex compared with untreated cells (Fig. 15). The increased SOD levels proved the an-

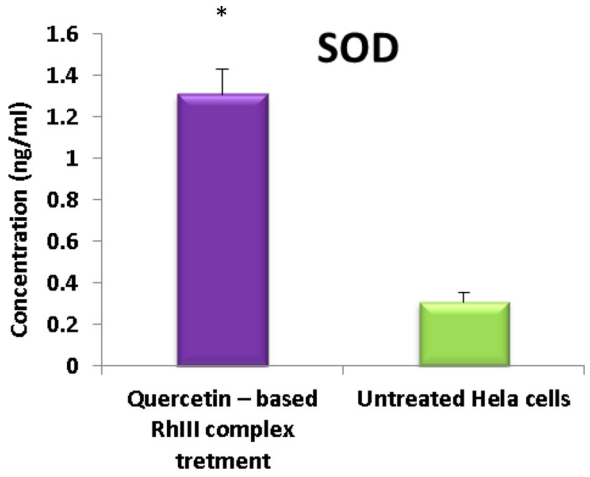

Fig. 15. SOD activity in Hela cells treated with the IC_{50} of the quercetin – based Rh^{III} complex. *displays significant difference ($P = 0.001$) compared with untreated Hela cells.

tioxidant activity of the quercetin – based Rh^{III} complex inside the cancer cells that can help in promoting apoptosis in Hela cells.

4. Conclusion

In conclusion, the polyphenolic 3,3′,4′,5,7-pentahydroxylflavone (quercetin) forms a mononuclear metal complex with rhodium(III) ion in a molar ratio of 1:2 metal to ligand. The analytical and spectroscopic investigations used demonstrated the mode of bonding between quercetin and Rh^{III}-center in the six-coordinated metal complex that exists in a distorted octahedral geometry. The structure of the current quercetin – based Rh^{III} complex was achieved by processing the PXRD data by the relevant Expo 2014 computer program based on the Rietveld-Refinement approach. The SOD-like activity of the present quercetin – based rhodium(III) complex was examined and the obtained results showed moderate activity compared to other M-SOD mimics containing d^6-metals. By analogy with the mechanism of action of the natural enzyme and its mimicry, a mechanism for the catalytic activity of the quercetin–based Rh^{III} complex has been proposed (scheme 1). The ability of the Rh(III) chelate to bind to DNA was examined by spectroscopic investigations which indicated the successful binding of the metallic complex of quercetin to DNA by a groove/electrostatic binding pattern with intrinsic binding constants K_b 2.76 × 10^6 M^{-1}. The anti-proliferative activity of the quercetin – based Rh^{III} complex was confirmed by preventing replication of different types of cancer cell lines. That anti-proliferative activities may be via the surface binding between the quercetin – based Rh^{III} complex and the cancer cell's DNA. Also, the safety of the quercetin – based Rh^{III} complex was confirmed with its high IC_{50} on the normal cell line. Moreover, apoptosis activation was promoted by the quercetin – based Rh^{III} complex. The apoptotic pathway of the our complex was proven via increasing the p53 levels together with inhibiting both *Bcl2* and MMP9, then activating caspase 9 which then cleaves caspase 3, leading to apoptosis triggering. Apoptosis activation led to cell cycle arrest at the pre-G1 phase that stops Hela cell proliferation, which appeared in the decreased G2/M phase. Another proposed anticancer pathway that the quercetin – based Rh^{III} complex has antioxidant activity appeared in high DPPH value, SOD-like activity and elevated SOD levels in treated cells. That antioxidant activity can remove the excess ROS from the cancer cell preventing DNA mutation and stopping the cancer cell's proliferation and stimulating apoptotic cell death.

From the current data one can conclude that the quercetin – based Rh^{III} complex could be a promising anti-proliferative agent with low toxicity on normal cells, but *in vivo* studies must be done to confirm its safety on vital organs as well as its anticancer activity.

Declaration of Competing Interest

The authors declare that there are no conflicts of interest regarding the publication of this research paper.

Acknowledgements

This work was funded by Taif University Researchers Supporting Project number (TURSP-2020/222), Taif University, Taif, Saudi Arabia

Supplementary materials

Supplementary material associated with this article can be found, in the online version, at doi:10.1016/j.molstruc.2022.132584.

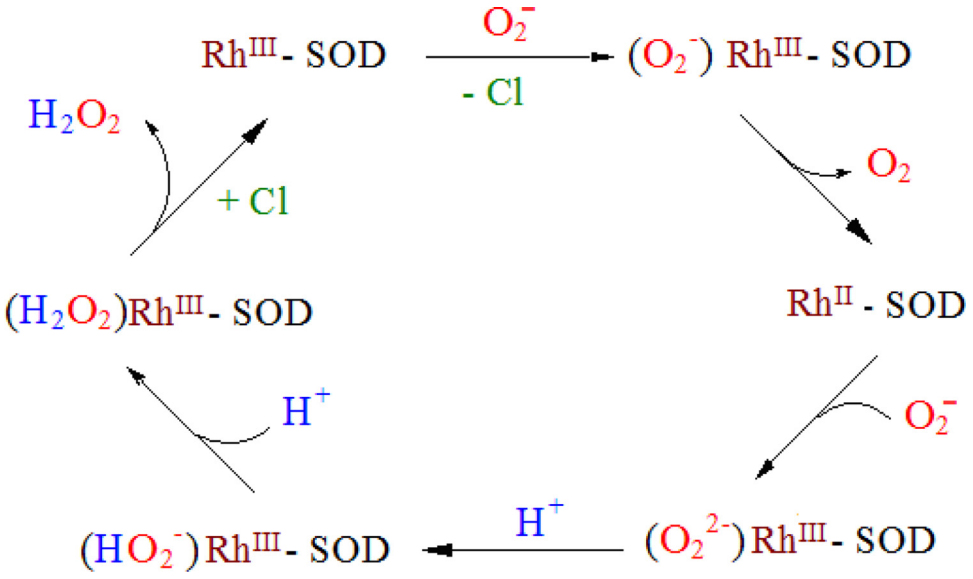

Scheme 1. Catalytic cycle of scavenging of $O_2^{\bullet -}$ by quercetin–based Rh^{III} complex; $[Rh^{III}L_2ClH_2O]$ is represented by Rh^{III}–SOD.

References

[1] S.P. Dunuweera, R.M.G. Rajapakse, Discovery, chemistry, anticancer action and targeting of cisplatin, Int. J. Clin. Oncol. Cancer Res. (2017).

[2] D.P. Silver, A.L. Richardson, A.C. Eklund, Z.C. Wang, Z. Szallasi, Q. Li, N. Juul, C.O. Leong, D. Calogrias, A. Buraimoh, A. Fatima, R.S. Gelman, P.D. Ryan, N.M. Tung, A. De Nicolo, S. Ganesan, A. Miron, C. Colin, D.C. Sgroi, L.W. Ellisen, E.P. Winer, J.E. Garber, Efficacy of neoadjuvant cisplatin in triple-negative breast cancer, J. Clin. Oncol. (2010), doi:10.1200/JCO.2009.22.4725.

[3] S. Ithimakin, Cisplatin, pharmacology and clinical applications, Cisplatin Pharmacol. Clin. Uses Advers. Eff. (2012).

[4] P.M. Bruno, Y. Liu, G.Y. Park, J. Murai, C.E. Koch, T.J. Eisen, J.R. Pritchard, Y. Pommier, S.J. Lippard, M.T. Hemann, N.M. Author, A subset of platinum-containing chemotherapeutic agents kill cells by inducing ribosome biogenesis stress rather than by engaging a DNA damage response HHS Public Access Author manuscript, Nat. Med. (2017).

[5] S. Manohar, N. Leung, Cisplatin nephrotoxicity: a review of the literature, J. Nephrol. (2018), doi:10.1007/s40620-017-0392-z.

[6] Z.Y. Duan, G.Y. Cai, J.J. Li, X.M. Chen, Cisplatin-induced renal toxicity in elderly people, Ther. Adv. Med. Oncol. (2020), doi:10.1177/1758835920923430.

[7] L. Amable, Cisplatin resistance and opportunities for precision medicine, Pharmacol. Res. (2016), doi:10.1016/j.phrs.2016.01.001.

[8] H.A. Sahyon, A.A. El-Bindary, A.F. Shoair, A.A. Abdellatif, Synthesis and characterization of ruthenium(III) complex containing 2-aminomethyl benzimidazole, and its anticancer activity of in vitro and in vivo models, J. Mol. Liq. 255 (2018) 122–134, doi:10.1016/j.molliq.2018.01.140.

[9] S.A. Elsayed, S. Harrypersad, H.A. Sahyon, M.A. El-Magd, C.J. Walsby, Ruthenium(II)/(III) DMSO-based complexes of 2-aminophenyl benzimidazole with in vitro and in vivo anticancer activity, Molecules 25 (2020) 1–26, doi:10.3390/molecules25184284.

[10] D.L. Ma, M. Wang, Z. Mao, C. Yang, C.T. Ng, C.H. Leung, Rhodium complexes as therapeutic agents, Dalt. Trans (2016), doi:10.1039/c5dt04338g.

[11] J. Rodríguez-Corrales, J. Wang, B.S.J. Winkel, K.J. Brewer, Mechanistic Investigation into DNA Modification by a RuII,RhIII Bimetallic Complex, ChemBioChem (2018), doi:10.1002/cbic.201800369.

[12] M. Sohrabi, M. Saeedi, B. Larijani, M. Mahdavi, Recent advances in biological activities of rhodium complexes: their applications in drug discovery research, Eur. J. Med. Chem. (2021), doi:10.1016/j.ejmech.2021.113308.

[13] Y.B. Peng, C. Tao, C.P. Tan, P. Zhao, Mitochondrial targeted rhodium(III) complexes: synthesis, characterized and antitumor mechanism investigation, J. Inorg. Biochem. (2021), doi:10.1016/j.jinorgbio.2021.111400.

[14] J. Wang, J.J. Nie, P. Guo, Z. Yan, B. Yu, W. Bu, Rhodium(I) complex-based polymeric nanomicelles in water exhibiting coexistent near-infrared phosphorescence imaging and anticancer activity in vivo, J. Am. Chem. Soc. (2020), doi:10.1021/jacs.9b11013.

[15] H. Liang, T. Hao, C. Yin, X. Yang, H. Fu, X. Zheng, R. Li, D. Xiao, H. Chen, Cyclometalated Rhodium(III) Complexes Based on Substituted 2-Phenylpyridine Ligands: synthesis, Structures, Photophysics, Electrochemistry, and DNA-Binding Properties, Eur. J. Inorg. Chem. (2017), doi:10.1002/ejic.201700700.

[16] X. Lu, Y.M. Wu, J.M. Yang, F.E. Ma, L.P. Li, S. Chen, Y. Zhang, Q.L. Ni, Y.M. Pan, X. Hong, Y. Peng, Preparation of Rhodium(III) complexes with 2(1H)-quinolinone derivatives and evaluation of their in vitro and in vivo antitumor activity, Eur. J. Med. Chem. (2018), doi:10.1016/j.ejmech.2018.03.074.

[17] R. Esteghamat-Panah, H. Hadadzadeh, H. Farrokhpour, J. Simpson, A. Abdolmaleki, F. Abyar, Synthesis, structure, DNA/protein binding, and cytotoxic activity of a rhodium(III) complex with 2,6-bis(2-benzimidazolyl)pyridine, Eur. J. Med. Chem. (2017), doi:10.1016/j.ejmech.2016.11.005.

[18] R.K. Gupta, G. Sharma, R. Pandey, A. Kumar, B. Koch, P.Z. Li, Q. Xu, D.S. Pandey, DNA/protein binding, molecular docking, and in vitro anticancer activity of some thioether-dipyrrinato complexes, Inorg. Chem. (2013), doi:10.1021/ic401662d.

[19] K.M. Boyle, J.K. Barton, A family of rhodium complexes with selective toxicity toward mismatch repair-deficient cancers, J. Am. Chem. Soc. (2018), doi:10.1021/jacs.8b02271.

[20] K.M. Boyle, J.K. Barton, Targeting DNA mismatches with rhodium metalloinsertors, Inorganica Chim. Acta. (2016), doi:10.1016/j.ica.2016.01.021.

[21] T.M. Khan, N.S. Gul, X. Lu, R. Kumar, M.I. Choudhary, H. Liang, Z.F. Chen, Rhodium(III) complexes with isoquinoline derivatives as potential anticancer agents:: In vitro and in vivo activity studies, Dalt. Trans. (2019), doi:10.1039/c9dt01951k.

[22] S. Kumar, A.K. Pandey, Chemistry and biological activities of flavonoids: an overview, Sci. World J. 2013 (2013) 1–16, doi:10.1155/2013/162750.

[23] D. Staedler, E. Idrizi, B.H. Kenzaoui, L. Juillerat-Jeanneret, Drug combinations with quercetin: doxorubicin plus quercetin in human breast cancer cells, Cancer Chemother. Pharmacol. (2011), doi:10.1007/s00280-011-1596-x.

[24] M. Hashemzaei, A.D. Far, A. Yari, R.E. Heravi, K. Tabrizian, S.M. Taghdisi, S.E. Sadegh, K. Tsarouhas, D. Kouretas, G. Tzanakakis, D. Nikitovic, N.Y. Anisimov, D.A. Spandidos, A.M. Tsatsakis, R. Rezaee, Anticancer and apoptosis-inducing effects of quercetin in vitro and in vivo, Oncol. Rep. (2017), doi:10.3892/or.2017.5766.

[25] S. Ranganathan, D. Halagowder, N.D. Sivasithambaram, Quercetin suppresses twist to induce apoptosis in MCF-7 breast cancer cells, PLoS ONE (2015), doi:10.1371/journal.pone.0141370.

[26] J. Duo, G.G. Ying, G.W. Wang, L. Zhang, Quercetin inhibits human breast cancer cell proliferation and induces apoptosis via Bcl-2 and Bax regulation, Mol. Med. Rep. (2012), doi:10.3892/mmr.2012.845.

[27] M. Ezzati, B. Yousefi, K. Velaei, A. Safa, A review on anti-cancer properties of Quercetin in breast cancer, Life Sci. (2020), doi:10.1016/j.lfs.2020.117463.

[28] L.T. Nguyen, Y.H. Lee, A.R. Sharma, J.B. Park, S. Jagga, G. Sharma, S.S. Lee, J.S. Nam, Quercetin induces apoptosis and cell cycle arrest in triple-negative breast cancer cells through modulation of Foxo3a activity, Korean J. Physiol. Pharmacol. (2017), doi:10.4196/kjpp.2017.21.2.205.

[29] H. Zhang, M. Zhang, L. Yu, Y. Zhao, N. He, X. Yang, Antitumor activities of quercetin and quercetin-5',8-disulfonate in human colon and breast cancer cell lines, Food Chem. Toxicol. (2012), doi:10.1016/j.fct.2012.01.025.

[30] R. Ravichandran, M. Rajendran, D. Devapiriam, Antioxidant study of quercetin and their metal complex and determination of stability constant by spectrophotometry method, Food Chem. (2014), doi:10.1016/j.foodchem.2013.09.080.

[31] B.A. Lakshmi, J.Y. Bae, J.H. An, S. Kim, Facile design and spectroscopic characterization of novel bio-inspired Quercetin-conjugated tetrakis (dimethylsulfoxide)dichlororuthenium(II) complex for enhanced anticancer properties, Inorganica Chim. Acta. (2019), doi:10.1016/j.ica.2019.118989.

[32] H. Manman, C. Weilan, L. Zhimin, P. Liang, H. Lixia, C. Min, ESI-TOF MS analysis of complexes formed between quercetin and five metal ions in hot water and a study into their DNA cleavage activity, J. Inorg. Biochem. (2019), doi:10.1016/j.jinorgbio.2019.03.004.

[33] E. Jabeen, N.K. Janjua, S. Ahmed, I. Tahiri, M. Kashif, A. Javed, DNA binding interaction studies of flavonoid complexes of Cu(II) and Fe(II) and determination of their chemotherapeutic potential, Inorganica Chim. Acta. (2019), doi:10.1016/j.ica.2019.119048.

[34] E. Halevas, B. Mavroidi, M. Pelecanou, A.G. Hatzidimitriou, Structurally characterized zinc complexes of flavonoids chrysin and quercetin with antioxidant potential, Inorganica Chim. Acta. (2021), doi:10.1016/j.ica.2021.120407.

[35] G.A. Corrente, L. Malacaria, A. Beneduci, E. Furia, T. Marino, G. Mazzone, Experimental and theoretical study on the coordination properties of quercetin towards aluminum(III), iron(III) and copper(II) in aqueous solution, J. Mol. Liq. (2021), doi:10.1016/j.molliq.2020.115171.

[36] M.M. Ibrahim, M.A. El-Kemary, S.A. Al-Harbi, H.M. Al-Saidi, S.A. Sallam, A.E.M.M. Ramadan, Synthesis and Structural Characterization of Pyridine-based Mn(III), Fe(III), and Co(III) Complexes as SOD Mimics and BSA Binding Studies, J. Mol. Struct. (2021), doi:10.1016/j.molstruc.2020.129706.

[37] A.E.M.M. Ramadan, Macrocyclic nickel(II) complexes: synthesis, characterization, superoxide scavenging activity and DNA-binding, J. Mol. Struct. (2012), doi:10.1016/j.molstruc.2012.01.048.

[38] H.A. Sahyon, Sami Al-Harbi, Chemoprotective role of an extract of the heart of the Phoenix dactylifera tree on adriamycin-induced cardiotoxicity and nephrotoxicity by regulating apoptosis, oxidative stress and PD-1 suppression, Food Chem. Toxicol. (2020) https://doi.org/https://doi.org/10.1016/j.fct.2019.111045.

[39] T.W. Chung, S.C. Lin, J.H. Su, Y.K. Chen, C.C. Lin, H.L. Chan, Sinularin induces DNA damage, G2/M phase arrest, and apoptosis in human hepatocellular carcinoma cells, BMC Complement. Altern. Med. (2017), doi:10.1186/s12906-017-1583-9.

[40] A.H. Cory, T.C. Owen, J.A. Barltrop, J.G. Cory, Use of an aqueous soluble tetrazolium/formazan assay for cell growth assays in culture, Cancer Commun. (1991).

[41] S. Roy, R. Das, B. Ghosh, T. Chakraborty, Deciphering the biochemical and molecular mechanism underlying the in vitro and in vivo chemotherapeutic efficacy of ruthenium quercetin complex in colon cancer, Mol. Carcinog. (2018), doi:10.1002/mc.22792.

[42] S.B. Bukhari, S. Memon, M. Mahroof-Tahir, M.I. Bhanger, Synthesis, characterization and antioxidant activity copper-quercetin complex, Spectrochim. Acta - Part A Mol. Biomol. Spectrosc. (2009), doi:10.1016/j.saa.2008.07.030.

[43] A. Raza, X. Xu, L. Xia, C. Xia, J. Tang, Z. Ouyang, Quercetin-Iron complex: synthesis, characterization, antioxidant, DNA binding, DNA cleavage, and antibacterial activity studies, J. Fluoresc. (2016), doi:10.1007/s10895-016-1896-y.

[44] S. Birjees Bukhari, S. Memon, M. Mahroof Tahir, M.I. Bhanger, Synthesis, characterization and investigation of antioxidant activity of cobalt-quercetin complex, J. Mol. Struct. (2008), doi:10.1016/j.molstruc.2008.04.050.

[45] M. Kalinowska, G. Świderski, M. Matejczyk, W. Lewandowski, Spectroscopic, thermogravimetric and biological studies of Na(I), Ni(II) and Zn(II) complexes of quercetin, J. Therm. Anal. Calorim (2016), doi:10.1007/s10973-016-5362-5.

[46] J. Zhou, L. fang Wang, J. yi Wang, N. Tang, Synthesis, characterization, antioxidative and antitumor activities of solid quercetin rare earth(III) complexes, J. Inorg. Biochem. (2001), doi:10.1016/S0162-0134(00)00128-8.

[47] W.J. Orville-Thomas, Advanced inorganic chemistry, J. Mol. Struct. (1973), doi:10.1016/0022-2860(73)85197-x.

[48] K.R. Seddon, Infrared and Raman spectra of inorganic and coordination compounds, J. Organomet. Chem. (1987), doi:10.1016/0022-328x(87)80177-8.

[49] G. R, Inorganic electronic spectroscopy, J. Mol. Struct. (1985), doi:10.1016/0022-2860(85)80208-8.

[50] W.J. Geary, The use of conductivity measurements in organic solvents for the characterisation of coordination compounds, Coord. Chem. Rev. (1971), doi:10.1016/S0010-8545(00)80009-0.

[51] P.K. Bhattacharya, Electronic spectra of some rhodium(III) complexes of saturated cyclic tetramines, J. Chem. Soc. Dalt. Trans. (1980), doi:10.1039/DT9800000810.

[52] V.K. Sharma, S. Srivastava, A. Srivastava, Spectroscopic, thermal and biological studies on some trivalent ruthenium and rhodium NS chelating thiosemicarbazone complexes, Bioinorg. Chem. Appl. (2007), doi:10.1155/2007/68374.

[53] S. Chandra, R. Singh, Pd(II), Pt(II), Rh(III), Ir(III) & Ru(III) complexes of some nitrogen-oxygen donor ligands, Indian J. Chem. -Sect. A. (1988).

[54] E. Manessi-Zoupa, T.F. Zafiropoulos, S.P. Perlepes, Preparation and Properties of Rhodium(III) complexes with the tetradentate ligand N,N′-Bis(2'-pyridinecarboxamide)-l,8-naphthalene, Zeitschrift Fur Naturforsch. - Sect. B J. Chem. Sci. (1994), doi:10.1515/znb-1994-0118.
[55] A.C. Fabretti, C. Preti, L. Tassi, G. Tosi, P. Zannini, Dithiocarbamate complexes of rhodium(III), iridium(III), palladium(II) and platinum(II), Inorganica Chim. Acta (1987), doi:10.1016/S0020-1693(00)87120-0.
[56] A. Avdeef, J.P. Fackler, Structural Trends of Tris(acetylacetonate)-, Tris(tropolonate)-, and Other Tris(bidentate ligand)-Metal Complexes. Additional Comments on the Trigonal Twist and Ligand-Ligand Repulsions in "Octahedral" D3 Bidentate Ligand-Metal Complexes, Inorg. Chem. (1975), doi:10.1021/ic50150a053.
[57] D.L. Kepert, Stereochemistry of Tris(bidentate) Complexes, Inorg. Chem. (1972), doi:10.1021/ic50113a022.
[58] O. Iranzo, Manganese complexes displaying superoxide dismutase activity: a balance between different factors, Bioorg. Chem. (2011), doi:10.1016/j.bioorg.2011.02.001.
[59] L.Q. Chai, J.J. Huang, H.S. Zhang, Y.L. Zhang, J.Y. Zhang, Y.X. Li, An unexpected cobalt(III) complex containing a Schiff base ligand: synthesis, crystal structure, spectroscopic behavior, electrochemical property and SOD-like activity, Spectrochim. Acta - Part A Mol. Biomol. Spectrosc. (2014), doi:10.1016/j.saa.2014.04.127.
[60] T. Nagano, T. Hirano, M. Hirobe, Superoxide dismutase mimics based on iron in vivo, J. Biol. Chem. (1989), doi:10.1016/s0021-9258(18)60521-6.
[61] Biological inorganic chemistry: structure and reactivity, Choice Rev. Online. (2007), doi:10.5860/choice.44-6242.
[62] M.M. Milutinović, A. Rilak, I. Bratsos, O. Klisurić, M. Vraneš, N. Gligorijević, S. Radulović, Ž.D. Bugarčić, New 4′-(4-chlorophenyl)-2,2′:6′,2″-terpyridine ruthenium(II) complexes: synthesis, characterization, interaction with DNA/BSA and cytotoxicity studies, J. Inorg. Biochem. (2017), doi:10.1016/j.jinorgbio.2016.10.001.
[63] R.F. Pasternack, E.J. Gibbs, J.J. Villafranca, J.J. Villafranca, Interactions of porphyrins with nucleic acids, Biochemistry (1983), doi:10.1021/bi00292a024.
[64] J. Kljun, I. Bratsos, E. Alessio, G. Psomas, U. Repnik, M. Butinar, B. Turk, I. Turel, New uses for old drugs: attempts to convert quinolone antibacterials into potential anticancer agents containing ruthenium, Inorg. Chem. (2013), doi:10.1021/ic401220x.
[65] S. Mukhopadhyay, R.K. Gupta, R.P. Paitandi, N.K. Rana, G. Sharma, B. Koch, L.K. Rana, M.S. Hundal, D.S. Pandey, Synthesis, Structure, DNA/Protein binding, and anticancer activity of some half-sandwich cyclometalated Rh(III) and Ir(III) complexes, Organometallics (2015), doi:10.1021/acs.organomet.5b00475.
[66] L. Tjioe, A. Meininger, T. Joshi, L. Spiccia, B. Graham, Efficient plasmid DNA cleavage by copper(II) complexes of 1,4,7-triazacyclononane ligands featuring xylyl-linked guanidinium groups, Inorg. Chem. (2011), doi:10.1021/ic102301n.
[67] A. Wolfe, G.H. Shimer, T. Meehan, Polycyclic aromatic hydrocarbons physically intercalate into duplex regions of denatured DNA, Biochemistry 26 (1987) 6392–6396, doi:10.1021/bi00394a013.
[68] L. Pellerito, L. Nagy, Organotin(IV)n+ complexes formed with biologically active ligands: equilibrium and structural studies, and some biological aspects, Coord. Chem. Rev. (2002), doi:10.1016/S0010-8545(01)00399-X.
[69] K. Savithri, B.C.V. Kumar, H.K. Vivek, H.D. Revanasiddappa, Synthesis and Characterization of Cobalt(III) and Copper(II) Complexes of 2-((E)-(6-Fluorobenzo[d]thiazol-2-ylimino) methyl)-4-chlorophenol: DNA Binding and Nuclease Studies—SOD and Antimicrobial Activities, Int. J. Spectrosc. (2018), doi:10.1155/2018/8759372.
[70] C. Da Porto, S. Calligaris, E. Celotti, M.C. Nicoli, Antiradical properties of commercial cognacs assessed by the DPPH(.) test, J. Agric. Food Chem. 48 (2000) 4241–4245, doi:10.1021/jf000167b.
[71] J.J. Lemasters, T. Qian, C.A. Bradham, D.A. Brenner, W.E. Cascio, L.C. Trost, Y. Nishimura, A.L. Nieminen, B. Herman, Mitochondrial dysfunction in the pathogenesis of necrotic and apoptotic cell death, J. Bioenerg. Biomembr. 31 (1999) 305–319, doi:10.1023/A:1005419617371.
[72] S.Y. Proskuryakov, V.L. Gabai, Mechanisms of tumor cell necrosis, Curr. Pharm. Des. 16 (2010) 56–68, doi:10.2174/138161210789941793.
[73] E.T. Arung, B.D. Wicaksono, Y.A. Handoko, I.W. Kusuma, D. Yulia, F. Sandra, Anti-cancer properties of diethylether extract of wood from Sukun (Artocarpus altilis) in human breast cancer (T47D) cells, Trop. J. Pharm. Res. (2009), doi:10.4314/tjpr.v8i4.45223.
[74] J.A. Pietenpol, Z.A. Stewart, Cell cycle checkpoint signaling: cell cycle arrest versus apoptosis, Toxicology (2002), doi:10.1016/S0300-483X(02)00460-2.
[75] T. Li, N. Kon, L. Jiang, M. Tan, T. Ludwig, Y. Zhao, R. Baer, W. Gu, Tumor suppression in the absence of p53-mediated cell-cycle arrest, apoptosis, and senescence, Cell (2012), doi:10.1016/j.cell.2012.04.026.
[76] S.P. Hussain, J. Schwank, F. Staib, X.W. Wang, C.C. Harris, TP53 mutations and hepatocellular carcinoma: insights into the etiology and pathogenesis of liver cancer, Oncogene (2007), doi:10.1038/sj.onc.1210279.
[77] D. Dhar, L. Antonucci, H. Nakagawa, J.Y. Kim, E. Glitzner, S. Caruso, S. Shalapour, L. Yang, M.A. Valasek, S. Lee, K. Minnich, E. Seki, J. Tuckermann, M. Sibilia, J. Zucman-Rossi, M. Karin, Liver cancer initiation requires p53 inhibition by CD44-enhanced growth factor signaling, Cancer Cell (2018), doi:10.1016/j.ccell.2018.05.003.
[78] Y. Guan, Q. He, Z. La, Roles of p53 in carcinogenesis, diagnosis and treatment of hepatocellular carcinoma, J. Cancer Mol. (2006).
[79] A.R.D. Delbridge, A. Strasser, The BCL-2 protein family, BH3-mimetics and cancer therapy, Cell Death Differ. (2015), doi:10.1038/cdd.2015.50.
[80] A.V. Vaseva, U.M. Moll, The mitochondrial p53 pathway, Biochim. Biophys. Acta - Bioenerg. (2009), doi:10.1016/j.bbabio.2008.10.005.
[81] S. Sajadimajd, R. Bahramsoltani, A. Iranpanah, J. Kumar Patra, G. Das, S. Gouda, R. Rahimi, E. Rezaeiamiri, H. Cao, F. Giampieri, M. Battino, R. Tundis, M.G. Campos, M.H. Farzaei, J. Xiao, Advances on natural polyphenols as anticancer agents for skin cancer, Pharmacol. Res. (2020), doi:10.1016/j.phrs.2019.104584.
[82] T. Ozaki, A. Nakagawara, Role of p53 in cell death and human cancers, Cancers (Basel) (2011), doi:10.3390/cancers3010994.
[83] E.I. Deryugina, J.P. Quigley, Matrix metalloproteinases and tumor metastasis, Cancer Metastasis Rev. (2006), doi:10.1007/s10555-006-7886-9.
[84] M.D. Martin, L.M. Matrisian, The other side of MMPs: protective roles in tumor progression, Cancer Metastasis Rev. (2007), doi:10.1007/s10555-007-9089-4.
[85] J.M. Pellikainen, K.M. Ropponen, V.V. Kataja, J.K. Kellokoski, M.J. Eskelinen, V.M. Kosma, Expression of matrix metalloproteinase (MMP)-2 and MMP-9 in breast cancer with a special reference to activator protein-2, HER2, and prognosis, Clin. Cancer Res. (2004), doi:10.1158/1078-0432.CCR-04-1061.
[86] S. Zucker, J. Vacirca, Role of matrix metalloproteinases (MMPs) in colorectal cancer, Cancer Metastasis Rev. (2004), doi:10.1023/A:1025867130437.
[87] Y.J. Shin, J.H. Kim, The role of EZH2 in the regulation of the activity of matrix metalloproteinases in prostate cancer cells, PLoS ONE (2012), doi:10.1371/journal.pone.0030393.
[88] I.N. Lavrik, Caspases: pharmacological manipulation of cell death, J. Clin. Invest. 115 (2005) 2665–2672, doi:10.1172/JCI26252.
[89] A. Saraste, K. Pulkki, M. Kallajoki, K. Henriksen, M. Parvinen, L.-M. Voipio-Pulkki, Apoptosis in human acute myocardial infarction, Circulation 95 (1997) 320–323.
[90] T. Kataoka, M. Schröter, M. Hahne, P. Schneider, M. Irmler, M. Thome, C.J. Froelich, J. Tschopp, FLIP prevents apoptosis induced by death receptors but not by perforin/granzyme B, chemotherapeutic drugs, and gamma irradiation, J. Immunol. 161 (1998) 3936–3942.
[91] M. Brentnall, L. Rodriguez-Menocal, R.L. De Guevara, E. Cepero, L.H. Boise, Caspase-9, caspase-3 and caspase-7 have distinct roles during intrinsic apoptosis, BMC Cell Biol. (2013), doi:10.1186/1471-2121-14-32.
[92] J.F.R. Kerr, History of the events leading to the formulation of the apoptosis concept, Toxicology 181 (2002) 471–474.
[93] P. Storz, Reactive oxygen species in tumor progression, Front. Biosci. 10 (2005) 1881–1896 https://doi.org/1667 [pii].
[94] E. Panieri, M.M. Santoro, Ros homeostasis and metabolism: a dangerous liason in cancer cells, Cell Death Dis. (2016), doi:10.1038/cddis.2016.105.
[95] M.J. O'Neil, The Merck Index: an encyclopedia of chemicals, Drugs, Biol. Drug Dev. Res. (2013), doi:10.1002/ddr.20159.
[96] K.J. Davies, Oxidative stress, antioxidant defenses, and damage removal, repair, and replacement systems, IUBMB Life 50 (2000) 279–289, doi:10.1080/713803728.
[97] J. Ismy, S. Sugandi, D. Rachmadi, S. Hardjowijoto, A. Mustafa, The effect of exogenous superoxide dismutase (SOD) on caspase-3 activation and apoptosis induction in PC-3 prostate cancer cells, Res. Rep. Urol. (2020), doi:10.2147/RRU.S271203.